Chapter 6

Lattices and positive quadratic forms

6.1 Introduction

Previous chapters were devoted to the study of lattices from the point of view of their symmetry and their Voronoï and Delone cells. This analysis was done essentially without explicit introduction of the basis in the ambient Euclidean space, E^n. Now we return to the study of lattices through associated positive quadratic forms. This approach requires us to introduce initially a lattice basis and to represent the translation lattice Λ^n in this basis

$$\Lambda^n := \{\mathbf{t}|\mathbf{t} = t_1\vec{b}_1 + \cdots + t_n\vec{b}_n, \; t_i \in \mathbb{Z}\}. \tag{6.1}$$

Here $\{\vec{b}_i\}$ is a basis of E^n. From the associated scalar products one can form the Gram matrix Q:

$$q_{ij} = (b_i, b_j); \quad Q = BB^\top = Q^\top. \tag{6.2}$$

Using the dual basis, defined in section 3.4 we obtain

$$Q(L^*) = Q(L)^{-1}. \tag{6.3}$$

We emphasize that the bases in the same orbit of the orthogonal group have the same Gram matrix; indeed $\forall S \in O_n$, $BS^\top(BS^\top)^\top = BS^\top SB^\top = BB^\top$, so Q describes the intrinsic lattice.

This symmetric matrix Q defines also a positive quadratic form $q(\vec{\ell})$ on E^n and, in particular on L, the lattice generated by the basis $\{\vec{b}_i\}$;

$$N(\vec{\ell}) = q(\vec{\ell}) := \sum_{i,j} \lambda_i q_{ij} \lambda_j, \tag{6.4}$$

where $\vec{\ell} = \sum_{i=1}^n \lambda_i \vec{b}_i$. Conversely, given the Gram matrix Q, one can reconstruct the intrinsic lattice.

Real quadratic forms in n variables and, equivalently, $n \times n$ real symmetric matrices Q, form a group under addition and they can be considered as elements of the vector space $\mathcal{Q}_n \sim \mathbb{R}^N$, where $N = n(n+1)/2$. This vector space $\mathcal{Q}_n$ carries a natural orthogonal scalar product $(Q, Q') = \text{tr}QQ' = \text{tr}Q'Q$. Since the sum of two positive quadratic forms is again a positive quadratic form, the set of n-variable positive quadratic forms is the interior $\mathcal{C}_+(\mathcal{Q}_n)$ of a convex closed cone $\overline{\mathcal{C}_+}(\mathcal{Q}_n)$. Notice that $\mathcal{C}_+(\mathcal{Q}_n)$ can be identified as the orbit space of the manifold $\mathcal{B}_n$ of bases under the action of the orthogonal group:

$$\mathcal{B}_n | O_n = GL_n(\mathbb{R}) : O_n = \mathcal{C}_+(\mathcal{Q}_n). \tag{6.5}$$

By a change of lattice basis, $\vec{b}'_i = \sum_j m_{ij}\vec{b}_j$, $M \in GL_n(\mathbb{Z})$, the Gram matrix Q is changed into the matrix:

$$Q \mapsto M.Q = MQM^\top. \tag{6.6}$$

So an intrinsic lattice corresponds to an orbit of $GL_n(\mathbb{Z})$ acting by (6.6) on $\mathcal{C}_+(\mathcal{Q}_n)$. The problem of choosing a fundamental domain for the $GL_n(\mathbb{Z})$ action on positive quadratic forms is equivalent to construction of the so called reduced forms. Also the overall scaling is unimportant for the study of intrinsic lattices. Therefore, it is possible to restrict analysis to appropriate sections of the cone, whose dimension is $n(n+1)/2 - 1$.

For two-dimensional lattices the corresponding cone of positive quadratic forms is three-dimensional, it can be easily visualized (see figure 6.1). Moreover, what we really need to look for in the case of quadratic forms in two variables is the two-dimensional section of the cone of positive quadratic forms represented, for example, in figure 6.2 where stratification of the cone is shown. Although the case of quadratic forms in two variables and associated two-dimensional lattices do not possess many complications arising for higher dimensional quadratic forms and lattices, it is quite instructive to study this particular case especially due to the possibility of visualization of corresponding structures.

6.2 Two dimensional quadratic forms and lattices

6.2.1 The $GL_2(\mathbb{Z})$ orbits on $\overline{\mathcal{C}}_+(\mathcal{Q}_2)$

The strata of the action of $GL_2(\mathbb{Z})$ on $\mathcal{C}_+(\mathcal{Q}_2)$ are the Bravais classes (see section 4.3 for initial definitions and chapter 8 for further details).

The three dimensional generic stratum represents the Bravais class $p2 = \mathbb{Z}_2$. After restriction to a section of the cone (see Figure 6.2) we see only a two-dimensional generic stratum.

Strata with stabilizers $p2mm$ and $c2mm$ are represented by one-dimensional lines on the section. On the whole cone of positive quadratic forms these strata are two-dimensional.
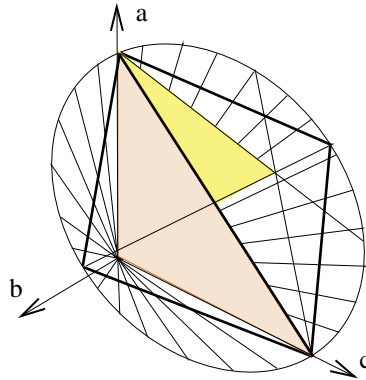
FIG. 6.1 – Representation of the cone of positive quadratic forms depending on two variables. Only interior points correspond to positive quadratic forms. The cone is divided into sub-cones with a given combinatorial type of Voronoï cell by planes passing through a vertex of the cone. One of such planes is shown by a dark shading. The cone is cut by the plane orthogonal to the axis. The traces of walls on this plane are shown by thick black lines. The number of walls is infinite and only a small number of walls is shown. Points on walls correspond to rectangular Voronoi cells. Generic points represent 2-dimensional lattices with the Voronoi cell being a parallelogon with six edges. Each generic region is further stratified by the action of the $GL(2, Z)$ group. The fundamental domain of $GL(2, Z)$ action consists of a sixth part of a generic domain together with its boundary. It is shown in figure as a lightly shaded region with its boundary.

From the partial ordering of Bravais classes (see section 4.4, Figures 4.6, 4.7) we know that $p4mm$ is generated by $p2mm$ and $c2mm$. Consequently, in Figure 6.2 the point at the intersection of $p2mm$ and $c2mm$ lines should correspond to a $p4mm$ Bravais class. For the 3d-cone, the $p4mm$ stratum is one-dimensional. It corresponds to intersections of the $p2mm$ and $c2mm$ planes. Similarly, the $p6mm$-invariant lattices appear at intersections of three $c2mm$ invariant strata. On Figure 6.2 the $p6mm$ stratum is shown as a system of isolated points whereas for the 3d-cone it is represented as a system of one-dimensional rays going through the cone vertex.

In order to construct the fundamental domain of the $GL_2(\mathbb{Z})$ action it is sufficient to choose one triangular domain (for example that shown in Figure 6.1 by light hatching) with its three boundaries but without a point belonging to the boundary of the cone.

Along with symmetry induced stratification of the cone of positive quadratic forms it is useful to look for a combinatorial classification of the Voronoï cells of corresponding lattices. We know that for two-dimensional lattices there are only two combinatorial types of Voronoï cells: hexagons for
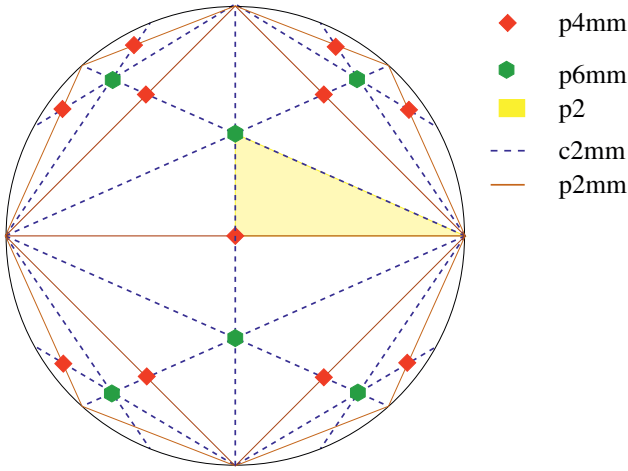
FIG. 6.2 – Representation of the section of the cone of positive quadratic forms depending on two variables. Stratification by the action of $GL(2, Z)$ into Bravais classes is shown. The fundamental domain includes a two-dimensional stratum (*p2* lattices); two one-dimensional strata (*c2mm* and *p2mm*); and two zero-dimensional strata (*p4mm* and *p6mm*),

the generic primitive case and rectangles for non-primitive case. Rectangular Voronoï cells are compatible only with *p2mm* and *p4mm* symmetry. This means that from the point of view of combinatorial classification big triangular domains in Figure 6.2 formed by *p2mm* boundary lines have in their interior points associated with primitive lattices (hexagon cells), whereas their boundaries (except vertices lying on the boundary of the cone) correspond to non-primitive lattices with rectangular Voronoï cells. Each such triangular domain consists of six fundamental regions of $GL_2(\mathbb{Z})$ action, intersecting at their boundaries.

6.2.2 Graphical representation of $GL_2(\mathbb{Z})$ transformation on the cone of positive quadratic forms

Remember that the action of a $GL_2(\mathbb{Z})$ element represented by matrix $B = \begin{pmatrix} b_{11} & b_{12} \\ b_{21} & b_{22} \end{pmatrix}$, satisfying condition $b_{11}b_{22} - b_{12}b_{21} = \pm 1$, on matrix $Q = \begin{pmatrix} q_{11} & q_{12} \\ q_{21} & q_{22} \end{pmatrix}$ is written as
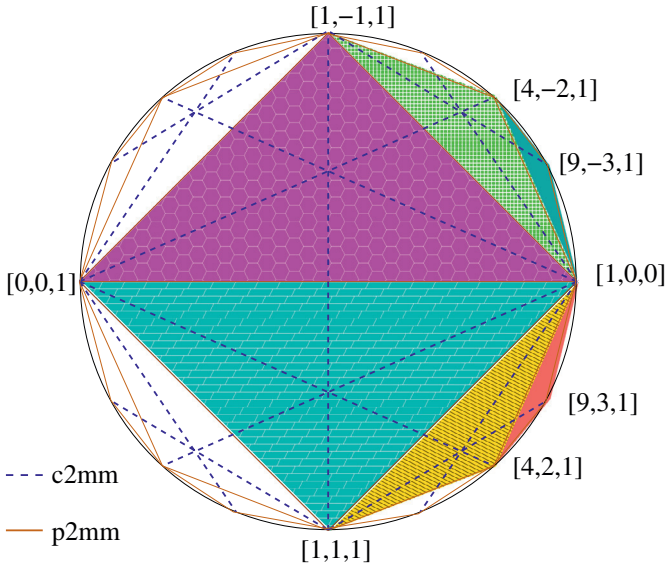
$$Q \to Q' = BQB^{\top}, \tag{6.7}$$

FIG. 6.3 – The action of B_1 transformation on the section of the cone of quadratic forms. Triangular domains shown by different shadings transform consecutively one into another in a clockwise direction around the point $[1, 0, 0]$ under B_1 action. Transformation of all other domains follows by applying the continuity arguments and invariance of combinatorial type under transformation. B_1^{-1} action corresponds to counterclockwise transformation of consecutive triangular domains around the same point $[1, 0, 0]$.

where $B^\top$ is the transposed matrix. The determinant of Q is invariant under $GL_2(\mathbb{Z})$ transformation. But on the representative section of the cone each point is denoted by the $[q_{11}, q_{12}, q_{22}]$ symbol which refers to the whole ray of quadratic forms with all possible determinants. The $[q_{11}, q_{12}, q_{22}]$ parameterization of points and lines used in Figures 6.3-6.5 is concretized in subsection 6.2.3 and Table 6.1.

$\quad$ $GL_2(\mathbb{Z})$ transformation is a continuous transformation of the disk representing the section of the cone of positive quadratic forms. Necessarily, it transforms each connected domain of one combinatorial (or symmetry) type into a domain of the same type and its boundaries into the respective boundaries. So to see the automorphism of the disk under the action of a concrete element of the $GL_2(\mathbb{Z})$ group, it is sufficient to study the transformation properties of special points being the vertices of domains of a given combinatorial type.
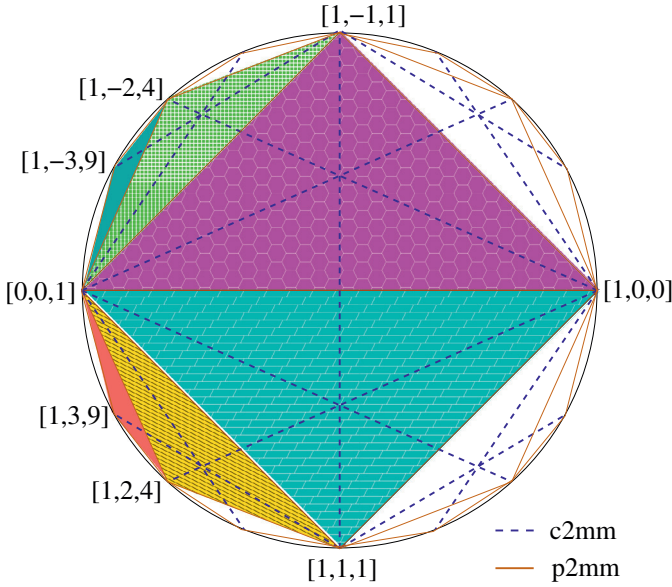
FIG. 6.4 – The action of B_2 transformation on the section of the cone of quadratic forms. Triangular domains shown by different shadings transform consecutively one into another in a clockwise direction around the point $[0, 0, 1]$ under B_2 action. Transformation of all other domains follows by applying the continuity arguments and invariance of combinatorial type under transformation.

Let us study the automorphism of the disk under the action of $B_1 = \begin{pmatrix} 1 & -1 \\ 0 & 1 \end{pmatrix}$ and its inverse $B_1^{-1} = \begin{pmatrix} 1 & 1 \\ 0 & 1 \end{pmatrix}$.

The point $[1, 0, 0]$ is invariant under B_1 action. The orbit of the point $[0, 0, 1]$ under the action of B_1 includes an infinite number of points which are obviously situated on the boundary of the disk

$$\begin{pmatrix} 1 & -1 \\ 0 & 1 \end{pmatrix}^K \begin{pmatrix} 0 & 0 \\ 0 & 1 \end{pmatrix} \begin{pmatrix} 1 & 0 \\ -1 & 1 \end{pmatrix}^K = \begin{pmatrix} K^2 & -K \\ -K & 1 \end{pmatrix}. \qquad (6.8)$$

Expression (6.8) is valid for any integer K value, positive or negative. From this transformation formula we see immediately that, for example, the triangle $([1, 0, 0], [0, 0, 1], [1, 1, 1])$ transforms under the action of B_1 into triangle $([1, 0, 0], [1, -1, 1], [0, 0, 1])$, then under the repeated action to triangle $([1, 0, 0], [4, -2, 1], [1, -1, 1])$, next to triangle $([1, 0, 0], [9, -3, 1], [4, -2, 1])$, etc. Figure 6.3 shows schematically these transformations.

In a similar way we can study the automorphism of the disk under the action of $B_2 = \begin{pmatrix} 1 & 0 \\ 1 & 1 \end{pmatrix}$ and its inverse $B_2^{-1} = \begin{pmatrix} 1 & 0 \\ -1 & 1 \end{pmatrix}$.

$$1 \rightarrow 4 : R_1; \quad 1 \rightarrow 2 : B_2\, R_0; \quad 1 \rightarrow 5 : R_1 B_2\, R_0;$$
$$1 \rightarrow 3 : B_2\, R_1 R_0; \quad 1 \rightarrow 6 : R_1 B_2 R_1 R_0.$$
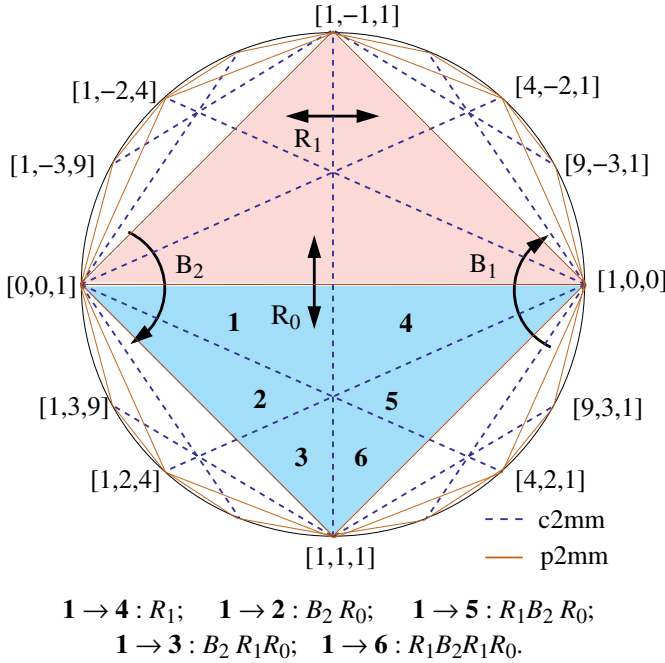
FIG. 6.5 – Examples of $GL_2(\mathbb{Z})$ elements realizing transformation between six equivalent sub-domains of the same connected combinatorial domain. Six sub-domains are labeled by big bold numbers $\mathbf{1}, \mathbf{2}, \mathbf{3}, \mathbf{4}, \mathbf{5}$, and $\mathbf{6}$.

Now the point $[0, 0, 1]$ is invariant under the B_2 action. The orbit of the point $[1, 0, 0]$ under the action of B_2 consists again in an infinite number of points situated on the boundary of the disk,

$$\begin{pmatrix} 1 & 0 \\ 1 & 1 \end{pmatrix}^K \begin{pmatrix} 1 & 0 \\ 0 & 0 \end{pmatrix} \begin{pmatrix} 1 & 1 \\ 0 & 1 \end{pmatrix}^K = \begin{pmatrix} 1 & K \\ K & K^2 \end{pmatrix}. \qquad (6.9)$$

Expression (6.9) allows us to construct a graphical visualization of the B_2 transformation shown in Figure 6.4 and to see, in particular, that the triangle $([0, 0, 1], [1, 0, 0], [1, -1, 1])$ transforms under B_2 action into triangle $([0, 0, 1], [1, 1, 1], [1, 0, 0])$, then under the repeated action to triangle $([0, 0, 1], [1, 2, 4], [1, 1, 1])$, next to triangle $([0, 0, 1], [1, 3, 9], [1, 2, 4])$, etc.

Along with transformation of points we can directly analyze transformation of lines. For example, we can find the image of the line $q_{12} = 0$ (corresponding to the $p2mm$ invariant boundary between generic combinatorial domains) under the action of B_2^K,

$$\begin{pmatrix} 1 & 0 \\ K & 1 \end{pmatrix} \begin{pmatrix} q_{11} & 0 \\ 0 & q_{22} \end{pmatrix} \begin{pmatrix} 1 & K \\ 0 & 1 \end{pmatrix} = \begin{pmatrix} q_{11} & K q_{11} \\ K q_{11} & K^2 q_{11} + q_{22} \end{pmatrix}. \qquad (6.10)$$

TAB. 6.1 – $[q_{11}, q_{12}, q_{22}]$ parameterization of several lines on the section of cone of positive quadratic forms together with points lying on them and the combinatorial type of corresponding Voronoï cell.

Line	Points on line	Combinatorial type
$q_{12} = 0$	$[0, 0, 1]$; $[1, 0, 0]$	4-cell
$q_{12} - q_{11} = 0$	$[0, 0, 1]$; $[1, 1, 1]$	4-cell
$q_{12} - q_{22} = 0$	$[1, 0, 0]$; $[1, 1, 1]$	4-cell
$q_{12} + q_{11} = 0$	$[0, 0, 1]$; $[1, -1, 1]$	4-cell
$q_{12} + q_{22} = 0$	$[1, 0, 0]$; $[1, -1, 1]$	4-cell
$q_{12} - 2q_{11} = 0$	$[0, 0, 1]$; $[1, 2, 4]$	4-cell
$q_{12} - 2q_{22} = 0$	$[1, 0, 0]$; $[4, 2, 1]$	4-cell
$q_{12} + 2q_{11} = 0$	$[0, 0, 1]$; $[1, -2, 4]$	4-cell
$q_{12} + 2q_{22} = 0$	$[1, 0, 0]$; $[4, -2, 1]$	4-cell
$q_{11} - 3q_{12} + 2q_{22} = 0$	$[1, 1, 1]$; $[4, 2, 1]$	4-cell
$2q_{11} - 3q_{12} + q_{22} = 0$	$[1, 1, 1]$; $[1, 2, 4]$	4-cell
$q_{11} + 3q_{12} + 2q_{22} = 0$	$[1, -1, 1]$; $[4, -2, 1]$	4-cell
$2q_{11} + 3q_{12} + q_{22} = 0$	$[1, -1, 1]$; $[1, -2, 4]$	4-cell
$2q_{12} - q_{11} = 0$	$[0, 0, 1]$; $[4, 2, 1]$	6-cell
$2q_{12} - q_{22} = 0$	$[1, 0, 0]$; $[1, 2, 4]$	6-cell
$2q_{12} + q_{11} = 0$	$[0, 0, 1]$; $[4, -2, 1]$	6-cell
$2q_{12} + q_{22} = 0$	$[1, 0, 0]$; $[1, -2, 4]$	6-cell

This means that the line $q_{12} = 0$ transforms under the action of B_2^K into the line $q_{12} = Kq_{11}$. This allows us to easily label all boundaries between different combinatorial domains going through the $[0, 0, 1]$ fixed point of B_2 action.

Obviously, one can apply the same transformation to lines which are boundaries between different fundamental domains of $GL_2(\mathbb{Z})$ action but which correspond to the primitive combinatorial type ($c2mm$ invariant lines). For example, for the $q_{11} - 2q_{12} = 0$ line we get

$$\begin{pmatrix} 1 & 0 \\ K & 1 \end{pmatrix} \begin{pmatrix} 2q_{12} & q_{12} \\ q_{12} & q_{22} \end{pmatrix} \begin{pmatrix} 1 & K \\ 0 & 1 \end{pmatrix} = \begin{pmatrix} 2q_{12} & (2K+1)q_{12} \\ (2K+1)q_{12} & 2K(K+1)q_{12} + q_{22} \end{pmatrix}. \tag{6.11}$$

To see other important $GL_2(\mathbb{Z})$ transformations we need to add two reflections. The reflection $R_0 = \begin{pmatrix} 1 & 0 \\ 0 & -1 \end{pmatrix}$ corresponds to a reflection in the $q_{12} = 0$ line. It reverses the sign of q_{12}. Another reflection, $R_1 = \begin{pmatrix} 0 & 1 \\ 1 & 0 \end{pmatrix}$ interchanges q_{11} and q_{22}. It may be geometrically seen as reflection in the $q_{12} = 0$ line.

The action of four elements B_0, B_1, R_0, R_1 on the section of cone of quadratic forms is shown schematically in Figure 6.5. Using their geometrical visualization it is easy to find some simple sequences of transformations
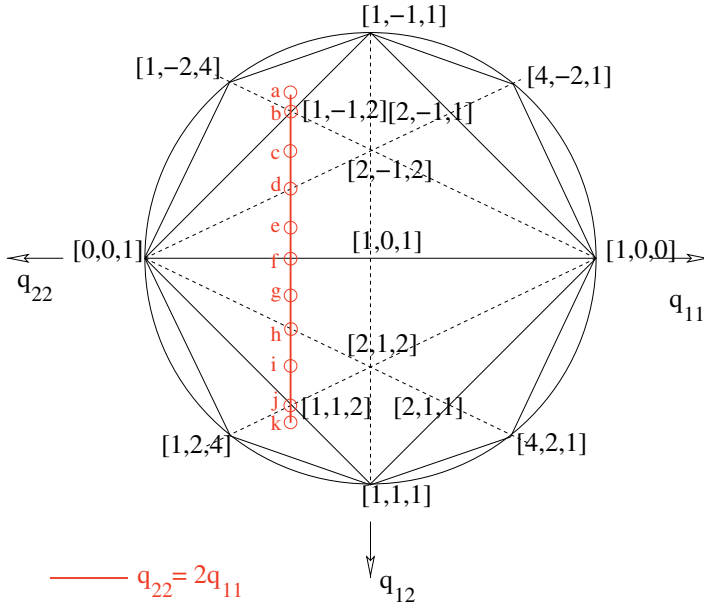
FIG. 6.6 – Section of the cone of quadratic forms with a path (a–k) along which evolution of lattices together with their Voronoï cell is shown in the next Figure 6.7. Notation for different lines is given in a separate Table 6.1.

which allow passage from one possible choice of fundamental domain to another one within the same domain of the combinatorial type. Examples of such transformations between six subdomains are given also in Figure 6.5.

6.2.3   Correspondence between quadratic forms and Voronoï cells

In order to see better the correspondence between points of the cone of positive quadratic forms and the corresponding Voronoï cell we take in figure 6.6 a series of points and represent in Figure 6.7 the evolution of the corresponding lattice and its Voronoï cell.

As we are interested not really in points of the cone but in rays, only two parameters are needed to define a ray. All matrices $Q = \begin{pmatrix} q_{11} & q_{12} \\ q_{12} & q_{22} \end{pmatrix}$ with different nonzero determinants but with the same ratio $q_{11} : q_{12} : q_{22}$ correspond to the same ray of the cone. Thus we can represent a ray by its projective coordinates $[q_{11}, q_{12}, q_{22}]$. Figure 6.6 shows stratification of the cone of positive quadratic forms in projective coordinates $[q_{11}, q_{12}, q_{22}]$. Equations for several lines corresponding to $c2mm$ and $p2mm$ strata are given in Table 6.1.
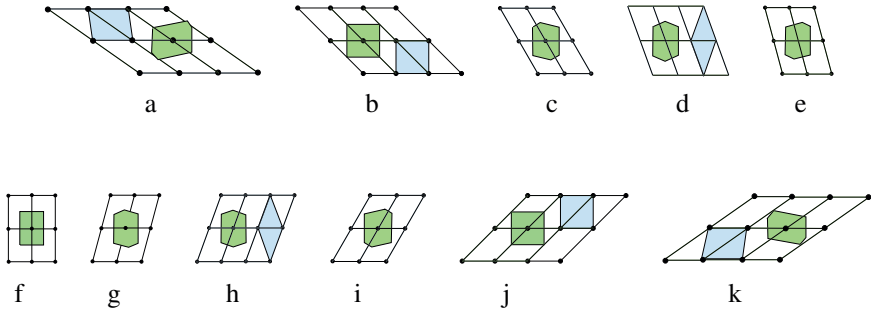
FIG. 6.7 – Lattices and their Voronoï cells associated with points on the section of the cone of positive quadratic forms shown in Figure 6.6.

As a path in the section of the cone of positive quadratic forms we take the line given by equation $q_{22} = 2q_{11}$. Along this line the 11 representative points $a, b, \ldots, k$ are chosen to cover different domains and to cross $c2mm$ and $p2mm$ strata. Lattices with their Voronoï cell for all these representative points are collected in Figure 6.7.

6.2.4 Reduction of two variable quadratic forms

To build a basis for a lattice L, we can start with any visible vector. We will choose a shortest vector $\vec{s}_1 \in S \subset L$; $\vec{s}_1$ defines a 1-sublattice $\{\mu \vec{s}_1; \ \mu \in \mathbb{Z}\}$. Then the 2-dimensional point lattice L becomes a union[1] $L = \cup_{\lambda \in \mathbb{Z}} \Sigma_\lambda$ of one-dimensional identical point lattices ("rangées") with $\Sigma_0 := \{\mu \vec{s}_1\}$ and $\Sigma_{\pm 1}$ its nearest "rangées". The second basis vector $\vec{s}_2$ should belong to $\Sigma_{\pm 1}$. These two rangées contain at least one vector whose orthogonal projection on the axis defined by $\vec{s}_1$ has the coordinate x which satisfies[2] $-\frac{1}{2} \leq x \leq 0$. When x satisfies the inequalities, we choose the corresponding vector as $\vec{s}_2$. The quadratic form defined by this basis is represented by the matrix with elements $q_{ij} = (\vec{s}_i, \vec{s}_j)$; these matrix elements satisfy exactly the conditions;

$$0 \leq -2q_{12} \leq q_{11} \leq q_{22}, \qquad 0 < q_{11}. \qquad (6.12)$$

The set of quadratic forms defined by (6.12) is a fundamental domain of $\mathcal{C}_+(\mathcal{Q}_2)$: i.e. this domain contains one, and only one, quadratic form of each orbit of the $GL_2(\mathbb{Z})$ action on $\mathcal{C}_+(\mathcal{Q}_2)$.

---

[1] The arguments used here are those of [29]. Bravais wrote in French and used the words: "rangée, réseau, assemblage" for 1-, 2-, and 3-dimensional lattices, respectively. That makes his paper more colorful!

[2] The choice of the sign of x is arbitrary. We choose here the negative sign because this has a natural generalization to arbitrary n.

Determining a fundamental domain on $\mathcal{C}_+(\mathcal{Q}_n)$ is known as the problem of arithmetic reduction of quadratic forms. For $n = 2$ it was first solved by Lagrange [65].

Another approach to classification of lattices and associated quadratic forms was introduced by Voronoï ([94], p.157) and developed later by Delone [42]. Using Lagrange reduction, we can always choose a basis of a lattice such that the coefficients of the associated quadratic form $q_{11}x^2 + 2q_{12}xy + q_{22}y^2$ satisfy (6.12) $0 \leq -2q_{12} \leq q_{11} \leq q_{22}, 0 < q_{11}$. With the variables $\lambda = q_{11}+q_{12}$, $\mu = q_{22} + q_{12}$, $\nu = -q_{12}$, the quadratic form becomes a sum of squares:

$$\lambda x^2 + \mu y^2 + \nu(x - y)^2, \quad \lambda \geq 0,\ \mu \geq 0,\ \nu \geq 0. \quad \det(q_{ij}) = \lambda\mu + \mu\nu + \nu\lambda > 0. \tag{6.13}$$

As the value of the determinant shows, the quadratic form is positive if no more than one of the three parameters vanishes. We have the norms:

$$N\begin{pmatrix}1\\0\end{pmatrix} = \lambda + \nu; \quad N\begin{pmatrix}0\\1\end{pmatrix} = \mu + \nu; \quad N\begin{pmatrix}1\\1\end{pmatrix} = \lambda + \mu; \tag{6.14}$$

there is a complete syntactic symmetry among the parameters λ, μ, ν. The domain in $\mathcal{C}_+(\mathcal{Q}_2)$ associated with generic lattices possessing a primitive (hexagon) combinatorial type of Voronoï cell is invariant by the group of permutations S_3 of the three parameters λ, μ, ν. Indeed, it corresponds to the triangle $[0, 0, 1]$, $[1, 0, 0]$, $[1, 1, 1]$ of Figure 6.6 and S_3 permutes the six fundamental domains contained in the domain of (6.13).

It is straightforward to describe the five Bravais strata by studying them in the parameter space $\mathcal{C}_+(\mathcal{Q}_2)$ with λ, μ, ν parameterization. They can be labeled by an elegant symbol invented by Delone: the three parameters are represented by the three sides of a triangle.

First case: $\lambda\mu\nu \neq 0$:

i) Generic Bravais class $p2$: represented by the Delone symbol $\triangle$

ii) When two parameters are equal, an order 2 symmetry appears: the invariance by R_1 in figure 6.6 (for instance $\lambda = \mu$); it exchanges the two equal sides of the triangle; it corresponds to the Bravais class $c2mm$: $\triangle$

iii) When the three parameters are equal: we have the full symmetry S_3 of the triangle; with the inversion through the origin (=rotation by π), one describes the hexagonal Bravais class $p6mm$: $\triangle$

Second case: one of the three parameters vanishes[3].

---

[3] If we choose $\nu = 0$ the quadratic form is diagonal (invariant by R_0 in Figure 6.6). The cases $\lambda = 0$ and $\mu = 0$ are obtained from the preceding one by transforming the quadratic form by the $SL_2(\mathbb{Z})$ matrices $\begin{pmatrix} 1 & 0 \\ -1 & 1 \end{pmatrix}$ and $\begin{pmatrix} 1 & -1 \\ 0 & 1 \end{pmatrix}$ respectively.

i) The two other parameters are different: Bravais class $p2mm$

ii) The two other parameters are equal: Bravais class $p4mm$

An extension of Delone classification to higher dimensional lattices and quadratic forms results in more fine classification of lattices than simply combinatorial or symmetry (Bravais) classification. (See Delone classification of three-dimensional lattices in Chapter 8, section 8.5 and the representation of combinatorial types of lattices by graphs in section 6.7.)

6.3 Three dimensional quadratic forms and 3D-lattices

The set of 3-dimensional quadratic forms $\{q\}$ (corresponding to symmetric real 3×3 matrices Q) forms a 6-dimensional real vector space $\mathbb{R}^6$, with the scalar product $(Q.Q') = \mathrm{tr}QQ'$. The 6-dimensional submanifold of positive forms, $\mathcal{C}_+(\mathcal{Q}_3)$, is the interior of a convex, homogeneous, self-dual[4] cone. Since each positive quadratic form represents a 3-dimensional Euclidean lattice, modulo position, it is interesting to partition $\mathcal{C}_+(\mathcal{Q}_3)$ both, into the 14 domains of Bravais classes, and the 5 domains of combinatorial types of Voronoï cells.

This would be very redundant, however, because the representation of an Euclidean lattice by a quadratic form depends on the choice of basis vectors, as we have seen during the analysis of a more simpler case of 2-dimensional quadratic forms in the preceding section.

To study the set of 3-dimensional lattices one has to consider only a fundamental domain of $\mathcal{C}_+(\mathcal{Q}_3)$ for the $GL_3(\mathbb{Z})$ action. To choose such a domain was a classical problem: the first solution was given by Seeber in 1831 [84]. The interior of such a domain can be chosen, using the main conditions for obtuse forms, to be:

$$0 < q_{11} \leq q_{22} \leq q_{33}, \ i \neq j : \ q_{ij} \leq 0; \ 2|q_{ij}| \leq q_{ii}; \ 2|q_{12}+q_{13}+q_{23}| \leq q_{11}+q_{22}. \tag{6.15}$$

On the boundary of that domain there occur only non-generic Bravais classes with still some redundancy, which are solved by the auxiliary conditions[5]. That domain is unbounded. Since we are interested in lattices up to a dilation, we can consider only a five dimensional (bounded) domain of the group $GL_3(\mathbb{Z}) \times \mathbb{R}_+^\times$. The most natural way to do it is to choose the intersection of the domain (6.15) by the hyperplane $\mathrm{tr}Q = c$, with c a positive constant. We shall choose $\mathrm{tr}Q = 3$ and call $T\mathcal{C}_+(\mathcal{Q}_3)$ this 5 dimensional bounded domain. However it is still difficult to draw its picture! For studying a

---

[4] Both Q and Q^{-1} are in the cone.
[5] $|q_{23}| \leq |q_{13}|$ if $q_{11} = q_{22}$; $\quad |q_{13}| \leq |q_{12}|$ if $q_{22} = q_{33}$; $\quad q_{12} = 0$ if $2|q_{23}| = q_{22}$; $q_{12} = 0$ if $2|q_{13}| = q_{11}$; $\quad q_{13} = 0$ if $2|q_{12}| = q_{11}$; $\quad q_{11} \leq |q_{12} + 2q_{13}|$ if $2|q_{12} + q_{13} + q_{23}| = q_{11} + q_{22}$.

3-dimensional picture, we have to restrict ourselves to a section of $T\mathcal{C}_+(\mathcal{Q}_3)$ by a well chosen 4-dimensional subspace of $\mathcal{C}_+(\mathcal{Q}_3)$. To check the dimension arguments we note that the $\mathcal{C}_+(\mathcal{Q}_3)$ space is 6-dimensional. If we intersect 6-dimensional space by a 5-dimensional ($T\mathcal{C}_+(\mathcal{Q}_3)$) and by a 4-dimensional subspaces, generically the intersection of 5-dimensional and 4-dimensional subspaces is 3-dimensional.

How to cut the maximal number of different Bravais class domains? There are four maximal Bravais classes:

$$Pm\bar{3}m, \quad Fm\bar{3}m, \quad Im\bar{3}m, \quad P6/mmm.$$

For the partial ordering of the set of Bravais classes there is a unique largest element (i.e. with largest symmetry), smaller than these four maximal classes; that is the Bravais class Mono C $= C2/m$, whose domain has dimension 4. We choose a group G belonging to the conjugacy class of the $C2/m$ subgroups of $GL_3(\mathbb{Z})$. We denote by $\mathcal{H} = \mathcal{Q}_3^G$ the 4-dimensional subspace of the G-invariant quadratic forms. Its intersection with the hyperplane of the trace 3 quadratic forms will define the Euclidean 3-plane of our model (Figures 6.8, 6.9). Figure 6.8 shows a fundamental domain of the Mono C $= C2/m$ Bravais class. Its boundary shows, with some redundancy the fundamental domains of the 10 Bravais classes which have a larger symmetry. Moreover, the model shows simultaneously parts of the 5 domains of combinatorial types of Voronoï cell represented in Figure 6.9.

6.3.1   Michel's model of the 3D-case

We start by describing the stratification of the suggested above 3-dimensional model into different strata corresponding to different Bravais classes and into different domains associated with different combinatorial types of Voronoï cell. Note that this 3D-model was designed by Louis Michel during his visits and lecturing in Smith College, Northampton (USA) and Technion, Haifa (Israel).

We give now the description of the model and reserve some hints for its construction till the end of this section.

The model is the tetrahedron $ABCD$ (see Figure 6.8). Four vertices, five edges (except for the edge $\overline{AD}$) and the facet ABC correspond to points representing quadratic forms with $\det Q = 0$. All internal points, internal points of the facet ABC and of the edge $\overline{AD}$ represent positive quadratic forms.

Stratification of the tetrahedron $ABCD$ into Bravais classes for three-dimensional lattices is shown in Figure 6.8. There are 0-, 1-, 2-, and 3-dimensional strata for eleven Bravais classes (among 14 existing for the 3D-case). They are summarized in the following table
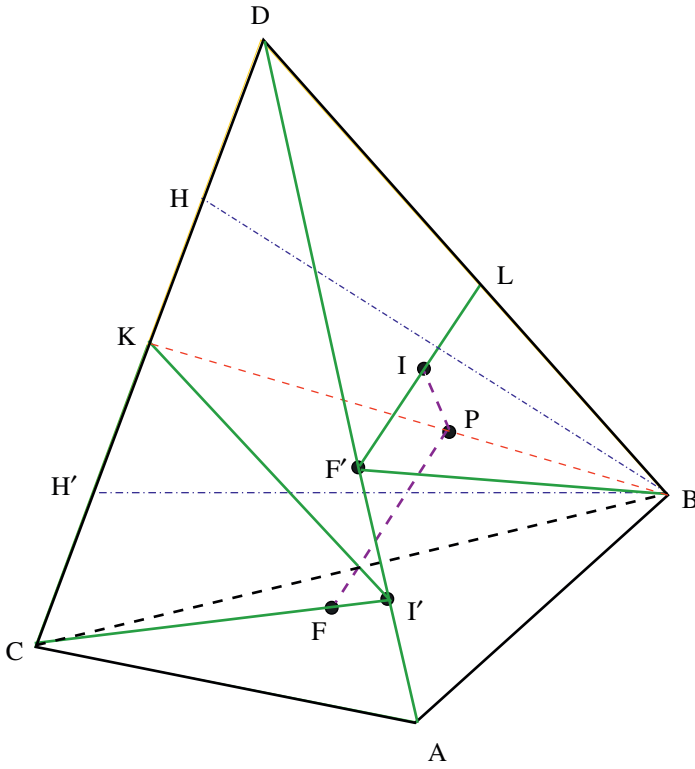
FIG. 6.8 – Partial model of the stratification of the cone of positive quadratic forms into Bravais classes for three-dimensional lattices. Strata of Bravais classes. Notice that $\det Q = 0$ on the facet ABC and on five edges of the tetrahedron, except for the edge $\overline{AD}$.

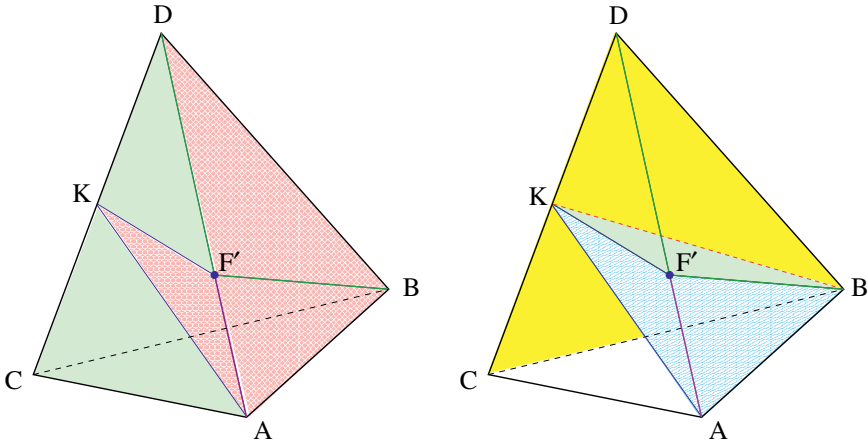|		
Mono C:	$C2/m$	interior of tetrahedron except intervals $\overline{PI}, \overline{PF}$;
Ort C:	$Cmmm$	facet BCD except $\overline{BH}, \overline{BH'}, \overline{BK}$;
Ort F:	$Fmmm$	facet BDA except $\overline{LF'}, \overline{BF'}$;
Ort I:	$Immm$	facet ACD except $\overline{KI'}, \overline{I'C}$;
Tet P:	$P4/mmm$	$\overline{BP}, \overline{PK}$;
Tet I:	$I4/mmm$	$\overline{BF'}, \overline{F'I}, \overline{IL}, \overline{DF'}, \overline{F'I'}, \overline{I'A}, \overline{KI'}, \overline{I'F}, \overline{FC}$;
Trig R:	$R\bar{3}m$	$\overline{PF}, \overline{PI}$;
Hex P:	$P6/mmm$	$\overline{BH}, \overline{BH'}$;
Cub P:	$Pm\bar{3}m$	P;
Cub F:	$Fm\bar{3}m$	F, F';
Cub I:	$Im\bar{3}m$	I, I'.

FIG. 6.9 – Partial model of the partition of the cone of positive quadratic forms into sub-cones of different combinatorial Voronoï cells. Notice that $\det Q = 0$ on the facet ABC and on five edges of the tetrahedron, except for the edge $\overline{AD}$. Left: Stratification of the facets ADB and ACD of the tetrahedron. Right: Strata non-visible on the left figure.

In order to visualize stratification of the tetrahedron $ABCD$ into domains of different combinatorial types we use in Figure 6.9 two images of the same tetrahedron and keep in this figure only points and lines important for stratification into combinatorial types. All points shown in Figure 6.9 are equally present in Figure 6.8, but some lines and planes present in Figure 6.8 are absent in Figure 6.9 because they have no specific combinatorial meaning. Remember that the lines and points absent in Figure 6.9 but present in Figure 6.8 are important to see the topology of the space of orbits (redundancy).

The stratification of the tetrahedron by different combinatorial types of Voronoï cell is given in the following table

14.24: interior of $DBF'K$ and $ABF'K$;
            interior of DBF', $BF'A$, and $F'KA$;
            interval $\overline{AF'}$
12.18: interior of $BACK$,
            interior of $BF'K$, DKF', and CKA;
            intervals $\overline{BF'}$ and $\overline{F'D}$
12.14: interior of ABK;
            intervals $\overline{KF'}$ and $\overline{KA}$;
            point F'
8.12:   facet BCD except $\overline{BK}$
6.8:   interval $\overline{BK}$

In order to see better the relation of the 3D-model to the six-dimensional cone of positive quadratic forms of three variables we recall below the relevant data for different combinatorial types of Voronoï cell and also on the dimension of these domains in the five-dimensional domain of positive quadratic forms with a given trace:

short notation	14.24	12.18	12.14	8.12	6.8
number of facet vectors	14	12	12	8	6
number of non-facet corona vectors	0	4	6	12	20
dimension of the domain in $T\mathcal{C}_+(\mathcal{Q}_3)$	5	4	3	3	2
dimension of the domain in model	3	3	2	2	1

6.3.2 Construction of the model

Now we return briefly to some points important for the construction of the described above model.

The 4 element group $G = \mathbb{Z}_2(r) \times \mathbb{Z}_2(-I)$, generated by the two matrices:

$$R = \begin{pmatrix} 0 & 1 & 0 \\ 1 & 0 & 0 \\ 0 & 0 & 1 \end{pmatrix}, \quad -I = \begin{pmatrix} -1 & 0 & 0 \\ 0 & -1 & 0 \\ 0 & 0 & -1 \end{pmatrix} \tag{6.16}$$

is a realization in $GL_3(\mathbb{Z})$ of the point symmetry of the monoclinic $C2/m$ lattices. Its invariant quadratic forms form the 4-dimensional space:

$$\mathcal{H} \equiv \mathcal{Q}_3^G = \left\{ Q = \begin{pmatrix} u & x & y \\ x & u & y \\ y & y & v \end{pmatrix}, \quad u, v, x, y \in \mathbb{R} \right\}. \tag{6.17}$$

In $\mathcal{H}$, the hyperplane of the trace 3 quadratic forms is:

$$\mathcal{H}' := \left\{ Q(x, y, z) = \begin{pmatrix} 1-z & x & y \\ x & 1-z & y \\ y & y & 1+2z \end{pmatrix} \right\}, \tag{6.18}$$

i.e. $2u + v = 3$, $v - u = 3z$. Given two quadratic forms $q, q' \in \mathcal{H}'$, their Euclidean distance is the square root of:

$$\mathrm{tr}(Q - Q')^2 = 2\big((x - x')^2 + 2(y - y')^2 + 3(z - z')^2\big). \tag{6.19}$$

The positive quadratic forms of $\mathcal{H}'$ form a bounded domain whose boundary is given by the condition for the quadratic forms of (6.18) to be positive:

$$-\frac{1}{2} < z < 1, \quad -(1-z) < x < 1 - z, \quad y^2 < (1 + x - z)(1 + 2z)/2. \tag{6.20}$$

In $\mathcal{H}'$ this is a convex domain $\mathcal{K}$ bounded by three planes and one sheet of a (two sheet) hyperbolic quadric.

By construction of $\mathcal{H}$, all G-invariant lattices are represented in it: those are all lattices of the Bravais classes $\geq$ Mono C $= C2/m$. We denote by N the stabilizer of $\mathcal{H}$ in the linear action of $GL_3(\mathbb{Z})$ on the space $\mathcal{Q}_3$. It is easy to prove that N is the normalizer $N_{GL_3(\mathbb{Z})}(G)$, i.e. the largest subgroup of $GL_3(\mathbb{Z})$ containing G as the invariant subgroup. The lattices of the Bravais classes $\geq$ Mono C are represented by the orbits of N inside $\mathcal{H} \cap \mathcal{C}_+(\mathcal{Q}_3)$. The represented Bravais classes correspond to the strata of this action; the stratum representing the smallest class, Mono C, is open dense and we want to choose a fundamental domain in it. For this we have first to determine N.

We notice that G is in the center of N. Since $G \triangleleft N$, every $n \in N$ has to conjugate the 4 matrices of G into each other; since the matrices of G have different traces, n commutes with them. So N is the centralizer of G in $GL_3(\mathbb{Z})$:

$$N = C_{GL_3(\mathbb{Z})}(G). \tag{6.21}$$

To compute this centralizer, it is sufficient to find the integral matrices n which satisfy $nr = rn$, $r \in G$, and require their determinant to be ± 1:

$$n = \begin{pmatrix} \alpha & \beta & \delta \\ \beta & \alpha & \delta \\ \delta' & \delta' & \gamma \end{pmatrix}, \quad \det n = (\alpha - \beta)\big(\gamma(\alpha + \beta) - 2\delta\delta'\big). \tag{6.22}$$

Each factor of the determinant should be ± 1:

$$\varepsilon^2 = 1, \quad \eta^2 = 1, \quad \alpha - \beta = \varepsilon, \quad \gamma(\alpha + \beta) - 2\delta\delta' = \eta. \tag{6.23}$$

One can prove that N is generated by the matrices

$$-I, \ R, \ S = \begin{pmatrix} 1 & 0 & 0 \\ 0 & 1 & 0 \\ 0 & 0 & -1 \end{pmatrix}, \ D = \begin{pmatrix} 1 & 0 & 1 \\ 0 & 1 & 1 \\ 0 & 0 & 1 \end{pmatrix}, \ D' = \begin{pmatrix} 1 & 0 & 0 \\ 0 & 1 & 0 \\ 1 & 1 & 1 \end{pmatrix}. \tag{6.24}$$

The matrices $-I, R, S$, generate a group of the Bravais class Ort C $= Cmmm$. Each of the matrices D, D' generates an infinite cyclic group $(\sim \mathbb{Z})$. Since the stabilizer of any lattice is finite, the orbits of N in $\mathcal{H} \cap \mathcal{C}_+(\mathcal{Q}_3)$ are infinite. In general the action of $g \in N$ on $\mathcal{H}$ does not preserve the trace of quadratic forms; so we deduce the action of N on $\mathcal{H}'$ from the action on $\mathcal{H}$ by adding the stereographic projection normalizing the trace.

By construction, the matrices $-I, R$ act trivially on $\mathcal{H}$; the matrix S changes y into $-y$ (both in $\mathcal{H}$ and $\mathcal{H}'$); so from now on we make the convention:

$$\text{convention}: \quad y \leq 0. \tag{6.25}$$

In $\mathcal{H}'$, the intersection of the positivity domain (6.20) with the 2-plane $y = 0$ is chosen to be part of the boundary of our fundamental domain; its points represent lattices of the Bravais class $Cmmm$ or greater ones.

Finite subgroups of N are crystallographic point groups; therefore each one containing G as a strict subgroup will have a linear manifold of fixed points containing a domain of a larger Bravais class. To find the finite subgroups of N, we must first determine its elements of finite order. As for $GL_3(\mathbb{Z})$ their order can be only 1, 2, 3, 4, or 6. Elements of order 3 must have as eigenvalues the three cubic roots of 1, so their trace, $\tau := \operatorname{tr} n = 2\alpha + \gamma$, must be 0. That is impossible since we know that γ is odd [see (6.18)]. Hence N *has no elements of order 3 or 6* (the square of an element of order 6 would be of order 3). The equation $n^2 = 1$ yields the following conditions in addition to those of (6.23), and combined with them:

$$\gamma^2 + 2\delta\delta' = 1, \quad 2\alpha(\alpha - \varepsilon) + \delta\delta' = 0, \quad \delta(\tau - \varepsilon) = 0 = \delta'(\tau - \varepsilon). \quad (6.26)$$

Since the eigenvalues of these matrices are ± 1, their trace can be either -3 or ± 1. In the former case we find easily that $n = -I$. When the trace $\tau = \pm 1$ we must have $\tau + \det n = 0$ so

$$\tau = 2\alpha + \gamma = -\varepsilon\eta. \quad (6.27)$$

That, with the first two conditions of (6.26), yields $\eta = -1$. Notice that for elements of N which are four fold, $\varepsilon = \eta = 1$, so there are no elements of order 4 in N. That proves that in N, all non-trivial elements of finite order are of order 2. Hence, all finite subgroups of N have the structure $\mathbf{Z}_2^k$, and we know from the study of the finite subgroups of $GL_3(\mathbb{Z})$ that $k \leq 3$.

It is easy to verify that the largest finite subgroups of N represent three of the four conjugacy classes of $\mathbb{Z}_2^3$ subgroups in $GL_3(\mathbb{Z})$; explicitly, they can be generated by the matrices[6]:

$$Cmmm: \langle R, S, -I \rangle, \quad Fmmm: \langle R, W^\top, -I \rangle, \quad Immm: \langle R, W, -I \rangle, \quad (6.28)$$

with

$$W = \begin{pmatrix} 0 & 1 & 0 \\ 1 & 0 & 0 \\ -1 & -1 & -1 \end{pmatrix}. \quad (6.29)$$

The domains of these 3 Bravais classes are two-dimensional. We determine those invariants by the three matrix groups chosen in (6.28); they belong to the boundary of the fundamental domain that we have chosen to represent the Bravais class $C2/m$.

We recall now that given a subgroup G of $GL_3(\mathbb{Z})$ it is easy to verify that the linear map on the orthogonal space $\mathbb{R}^6$ (see [11], Chapter 7.3):

$$\mathcal{C}_+(\mathcal{Q}_3) \ni Q \mapsto |G|^{-1} \sum_{g \in G} g^\top Q g \quad (6.30)$$

---

[6] Among the different method for distinguishing the two point groups $Fmmm$ and $Immm$, the fastest one is the computation of their fixed points (i.e. their cohomology group $H^0(P, L)$) by their action on the lattice L: $Fmmm$ has four and $Immm$ two fixed points per unit cell.

is an orthogonal projector over the subspace of G-invariant quadratic forms. From (6.30) we obtain the equations of the 2-planes supporting boundaries of the fundamental domain in $\mathcal{H}'$ invariant by matrix groups in (6.28). The boundary of the positivity domain (6.20) also has a facet supported by a 2-plane. We define the 2-planes by

$$f_1 : y = 0; \quad f_2 : 1 - z + x + 2y = 0; \quad f_3 : 1 + 2z + 2y = 0; \quad f_4 : 1 - z - x = 0.$$

So the fundamental domain we have chosen in $\mathcal{H}'$ is a tetrahedron $ABCD$ whose facets are

$$Cmmm = BCD \subset f_1; \quad Fmmm = ABD \subset f_2; \quad Immm = ACD \subset f_3;$$
$$\text{positivity boundary } = ABC \subset f_4. \tag{6.31}$$

The coordinates x, y, z of its vertices are:

$$A = \left(\frac{3}{4}, -\frac{3}{4}, \frac{1}{4}\right), \quad B = (0, 0, 1), \quad C = \left(\frac{3}{2}, 0, -\frac{1}{2}\right), \quad D = \left(-\frac{3}{2}, 0, -\frac{1}{2}\right). \tag{6.32}$$

Notice that on the facet ABC and on five edges of the tetrahedron, $\det Q = 0$. This is not true for the edge $\overline{AD} = ABD \cap ACD$, so it represents the Bravais class Tet I $= I4/mmm$ or higher.

Now we pass to the analysis of the Bravais class domains of dimension 1 and 0 in $\mathcal{H}'$.

Besides the four orthorhombic Bravais classes[7] the Bravais class Trig R $= R\bar{3}m$ is also a minimal supergroup[8] of $C2/m$. Its domain has dimension 1; indeed in $GL_3(\mathbb{Z})$ there are two groups of the conjugacy class $R\bar{3}m$ which contains $G \sim C2/m$ defined in (6.16); these groups are generated by the matrices:

$$R\bar{3}m = \langle R, -I, T\rangle, \ R\bar{3}m' = \langle R, -I, S^{-1}TS\rangle, \text{ with } T = \begin{pmatrix} 0 & 1 & 0 \\ 0 & 0 & 1 \\ 1 & 0 & 0 \end{pmatrix}, \tag{6.33}$$

and the corresponding invariant subspaces in $\mathcal{H}'$ are defined by $z = 0$ and $x = y$ or $x = -y$, respectively. Hence in our figure (we want $y < 0$) the trigonal Bravais class $R\bar{3}m$ is represented by two open segments inside the tetrahedron: in the subspace $z = 0$,

$$-\frac{1}{3} < x < 0 \quad \text{when } x = y; \quad 0 < x < \frac{1}{2} \quad \text{when } x = -y. \tag{6.34}$$

Their boundary is made of 3 points representing the 3 minimal supergroups of $R\bar{3}m$, i.e. the three cubic Bravais classes: we call these points:

$$P = (0, 0, 0), \quad I = \left(-\frac{1}{3}, -\frac{1}{3}, 0\right), \quad F = \left(\frac{1}{2}, -\frac{1}{2}, 0\right). \tag{6.35}$$

---

[7] Ort P $= Pmmm$ is not represented on the figure; this is also the case of the two other Bravais classes: Mono P $= P2/m$ and Tric $= \bar{1}$.

[8] i.e. there is no Bravais class X which satisfies $C2/m < X < R\bar{3}m$.

Notice that the point I is invariant by the group $R\bar{3}m$, the point F by $R\bar{3}m'$ and the point P by both groups.

There are two Bravais classes directly greater than the Bravais class Ort C = $Cmmm$; those are Tet P = $P4/mmm$ and Hex P = $P6/mmm$. The representative domain of each is 1-dimensional and has to belong to the facet BCD of the tetrahedron.

The stabilizer in $GL_3(\mathbb{Z})$ of the 2-plane $y = 0$ is the normalizer $N_{GL_3(\mathbb{Z})}(Cmmm) = P4/mmm$ which belongs to the Bravais class Tet P. Since $Cmmm$ acts trivially, its normalizer (which is a subgroup of $O_3(\mathbb{Z})$) acts only through the quotient

$$(P4/mmm)/Cmmm \sim \mathbb{Z}_2.$$

This action must be the orthogonal symmetry through an axis and this invariant axis represents the Bravais class Tet P. To realize the action of this quotient we can choose for instance the diagonal matrix $\begin{pmatrix} -1 & 0 & 0 \\ 0 & 1 & 0 \\ 0 & 0 & 1 \end{pmatrix}$, (in $P4/mmm$ but not in $Cmmm$); it changes x into $-x$ and leaves z invariant. So Tet P = $P4/mmm$ is represented by:

$$P4/mmm \mapsto x = y = 0, \quad -\frac{1}{2} < z < 0 < z < 1 \equiv \,]\overline{BK}[\,\backslash o. \qquad (6.36)$$

Note that the point $x = y = z = 0 \equiv o$ is represented in Figure 6.8 as point P.

In a similar way for Hex P = $P6/mmm$ we have

$$P6/mmm \mapsto y = 0, \quad x = \pm(1-z)/2, \quad -\frac{1}{2} < z < 1 \equiv \,]\overline{BH}[\,\cup\,]\overline{BH'}. \quad (6.37)$$

The positions of the specified points H, H', K are given below

$$H = \left(-\frac{3}{4}, 0, -\frac{1}{2}\right), \quad H' = \left(\frac{3}{4}, 0, -\frac{1}{2}\right), \quad K = \left(0, 0, -\frac{1}{2}\right). \qquad (6.38)$$

We emphasize the redundancy in the facet BCD: when $x \neq 0$, the points $(\pm x, 0, z)$ represent the same lattice. In the boundary of the open segments defined in (6.36), only one point represents a Bravais class; that is $x = y = z = 0$ representing the Cub P class. This point (given in (6.35)) is common to the boundaries of the domains representing Tet P and Trig R, the two Bravais classes directly smaller than Cub P.

We noticed in 6.3.1 that no vertices and only one of the six edges of the tetrahedron represents a Bravais class: it is $]\overline{AD}[=]ABD \cap ACD[$, corresponding to $Fmmm \cap Immm$, which represents Tet P = $I4/mmm$.

This edge must also carry two points F' and I' representing the two Bravais classes Cub F and Cub I directly greater than Tet I. To find these points we can use again the same method as for the facet BCD representing Ort C = $Cmmm$.

The facet BDA represents Ort $F = Fmmm$; its stabilizer is

$$N_{GL_3(\mathbb{Z})}(Fmmm) = Fm\bar{3}m$$

belonging to the Cub F Bravais class. It acts on the plane as a linear representation of the quotient $Fm\bar{3}m/Fmmm \sim \mathcal{S}_3$. We can take as representative of this quotient in $Fm\bar{3}m$ a subgroup conjugate to $R\bar{3}m$ defined in (6.33); it is generated by the matrices:

$$R\bar{3}m'' = \langle -I, \quad R' = M^{-1}RM, \quad T' = M^{-1}TM \rangle, \tag{6.39}$$

with $M = \begin{pmatrix} 0 & 1 & -1 \\ -1 & 0 & 1 \\ 1 & 0 & 0 \end{pmatrix}$. Then, using (6.30) for this group we obtain the point representing Cub F:

$$F' = (0, -\frac{1}{2}, 0) \in \overline{AD}. \tag{6.40}$$

Using (6.33), we verify

$$Q_{F'} = M^\top S^\top Q_F SM. \tag{6.41}$$

The same group transforms the segment $\overline{AD}$ into two other ones $\overline{A'D'}$, $\overline{A''D''}$ defined by:

$$\overline{A'D'} \quad : \quad A' = (0, -\frac{3}{5}, -\frac{1}{5}), \quad D' = (0, 0, 1) = B; \tag{6.42}$$
$$\overline{A''D''} \quad : \quad A'' = (-1, 0, 0), \quad D'' = (1, -1, 0). \tag{6.43}$$

The segment parts $\overline{A'F}$ and $\overline{F'D''}$ are in $\mathcal{H}'$ but outside the tetrahedron. The segment $\overline{A''F'}$ contains the point I defined in (6.34). The orbit of this point for the group $R\bar{3}m''$ contains the two other points:

$$I' = (\frac{3}{10}, -\frac{3}{5}, \frac{1}{10}) \in \overline{AD}; \quad I'' = (0, -\frac{6}{11}, -\frac{1}{11}). \tag{6.44}$$

The points I' and F' are on the edge $\overline{AD}$, (which represents Tet I). The point I'' does not belong to the tetrahedron.

Similarly, the stabilizer of the facet ACD, which represents the Bravais class Ort I $= Immm$, has normalizer $N_{GL_3(\mathbb{Z})}(Immm) = Im\bar{3}m$ which belongs to the Bravais class Cub I. This class is represented by the $Im\bar{3}m$ invariant point I' (defined in (6.44)). Moreover that normalizer transforms $\overline{AD}$ into two other segments whose intersections with the facet ACD are $\overline{KI'}$ and $\overline{CI'}$.

Finally, similar to the case of the facet BCD representing the class Ort C, we notice the same type of redundancy for the facets BAD and CAD

representing respectively the Bravais classes Ort F and Ort I. Indeed the intermediate groups

$$Fmmm < I4/mmm < N_{GL_3(\mathbb{Z})}(Fmmm) = Fm\bar{3}m, \qquad (6.45)$$

$$Immm < I4/mmm < N_{GL_3(\mathbb{Z})}(Immm) = Im\bar{3}m, \qquad (6.46)$$

belong to the Bravais class Tet I $= I4/mmm$; they respectively leave invariant the segments $\overline{BF'} \subset BAD$ and $\overline{KI'} \subset CAD$ which both represent Tet I. We notice that the interior of the triangles $DLF' \subset BDA$, $I'CA \subset CDA$ are not redundant.

All the obtained information is used for the construction of Figure 6.8.

To take into account all redundancies for points on the boundary of the tetrahedron $ABCD$ and to see the topology of the fundamental domain, the following identification of domains of the boundary of the tetrahedron should be done:

- Triangle BKD should be identified with BKC.

- Triangle $F'LB$ should be identified with $F'LD$.

- Triangle $I'KC$ should be identified with $I'KD$.

This implies that the following identification of 1-dimensional and 0-dimensional subsets on the boundary of $ABCD$ should be done:

- BH should be identified with BH'.

- $I'F'$ should be identified with $I'F$.

- CF should be identified with DF' and with BF'.

- F should be identified with F'.

6.4 Parallelohedra and cells for N-dimensional lattices.

In this section we give a brief description of some important new features related to the combinatorial classification of lattices and to the associated cone of positive quadratic forms which appear for lattices in higher dimensional $d \geq 4$ space as compared to the cases of planar $d = 2$ and space $d = 3$ lattices studied earlier in this chapter.

First of all it is necessary to make the definition of the combinatorial type of polytopes and their labeling for arbitrary dimension more precise.

The k-faces of a polytope P are partially ordered with respect to inclusion. Together with the empty set $\{\emptyset\}$ the k-faces form the *face lattice* $\mathcal{L}(P)$. (See the definition of a lattice as a partial ordered set in appendix A.) For any

two faces F and F' of $\mathcal{L}(P)$, the least upper bound is given by the k-face $F_\vee \supset F \cup F'$ having the least k. The k-face $F_\vee$ is unique because otherwise there would exist a face $\tilde{F} := F_\vee \cap F'_\vee \supset F \cup F'$ and thus, k would not be minimal. The greatest lower bound is given by the l-face $F_\wedge = F \cap F'$.

Definition: combinatorial type Two polytopes P and P' are combinatorially equivalent, $P' \overset{\text{comb}}{\simeq} P$, and belong to the same combinatorial type, if there exist a combinatorial isomorphism $\tau : \mathcal{L}(P) \to \mathcal{L}(P')$.

The combinatorial type of P is denoted by the *short symbol* $\mathbf{N}_{(n-1)}.\mathbf{N}_0$. For different combinatorial types having the same short symbol, additional letter/number symbols A, a, B, b, ... are added to distinguish them. In particular, we denote by n_h the number of 2-faces of P which are hexagons. In many cases the short symbol with the addition of -n_h uniquely characterizes special sets of parallelotopes [11]. More generally, for any k, $1 < k < n$, let $d_i^{(k)}$ be the number of k-faces of P which have $f_i^{(k)}$ subordinated $(k-1)$-faces, $i = 1, \ldots, r$. The k-subordination symbol is defined by

$$f_{1_{d_1^{(k)}}}^{(k)} f_{2_{d_2^{(k)}}}^{(k)} \cdots f_{r_{d_r^{(k)}}}^{(k)},$$

with $f_1^{(k)} < f_2^{(k)} < \cdots < f_r^{(k)}$. We give a few easy examples. The 2-subordination symbol of the 3-dimensional cubooctahedron is $4_6 6_8$, which means that there are six quadrilateral facets (2-faces) and eight hexagonal facets (2-faces). The 4-dimensional cube has the 3-subordination symbol 6_8 (there are eight facets (3-faces) possessing each six 2-faces) and the 2-subordination symbol 4_{24} (there are 24 quadrilateral 2-faces).

In order to verify combinatorial equivalence, the k-subordination symbols are determined for $k = (n-1), \ldots, 2$. The concatenation of these k-subordination symbols is called a *subordination scheme*. The subordination scheme does not characterize a polytope uniquely in dimension $d \geq 3$, but it is sufficient for parallelotopes in $\mathbb{R}^n$ for at least $n \leq 7$. A unique characterization of a polytope obtained by the unified polytope scheme is described in [48].

As we have introduced in section 5.4, each vertex of a primitive parallelotope in E^n is determined by the intersection of n facets. Let $\{\vec{f}_{l_1}, \ldots, \vec{f}_{l_n}\}$, be the set of the corresponding facet vectors. These vectors are linearly independent and determine a sublattice of the lattice L of index $\omega(v)$. It was shown by Voronoï[94], §66 that the upper bound for the number of vertices is reached exactly if, for each vertex v of a primitive parallelotope, $\omega(v) = 1$. Ryšhkov and Baranovskii [83] gave upper bounds for the index $\omega(v)$.

Theorem 9 *For dimensions $n = 2, 3, 4, 5$, and 6 the maximal values of the index $\omega(v)$ are 1, 1, 1, 2, and 3, respectively.*

The index $\omega(v)$ has direct correlation to the number of vertices N_0 of a primitive parallelotope P. The primitive parallelotope with $\omega(v) = 1$ for each of its vertices is called the principal primitive. Voronoï have shown [94] that

the number of k-faces N_k, $0 \leq k \leq d$ of a parallelotope in E^d is

$$N_k \leq (d+1-k) \sum_{l=0}^{d-k} (-1)^{d-k-l} \binom{d-k}{l} (1+l)^d. \qquad (6.47)$$

For the number of facets ($k = d - 1$) equation (6.47) becomes an equality *for all primitive* parallelohedra

$$N_{d-1} = 2(2^d - 1) \quad \text{for primitive parallelohedra} \qquad (6.48)$$

and coincides with the upper bound in the inequality for the number of facets vectors given by Minkowski [78] for a d-dimensional parallelohedron:

$$2d \leq |\mathcal{F}| \leq 2(2^d - 1). \qquad (6.49)$$

The equality sign in (6.47) holds for principal primitive parallelohedra for any k.

  In particular, from (6.47) we immediately have the following estimations for the number of vertices N_0, edges N_1 and $(d-2)$-faces $N_{(d-2)}$, related to the number of belts, for d-dimensional parallelohedra

$$N_0 \leq (d+1)!, \quad N_1 \leq \frac{d}{2}(d+1)!, \quad N_{(d-2)} \leq 3\left(1 - 2^{(d+1)} + 3^d\right). \qquad (6.50)$$

The equalities in (6.50) hold only for principal primitive parallelohedra. We note here that primitive parallelohedra contain sixfold belts only. This allows the number of belts N_b for primitive parallelohedra to be expressed as $N_b = N_{(d-2)}/6$.

  Non-principal primitive parallelohedra exist for $d \geq 5$. They have the same number of facets as principal primitive parallelohedra but the number of k-faces with $k \leq d - 2$ is less (for some k) than the maximal possible value for principal primitive parallelohedra.

  The number of combinatorial types of primitive parallelohedra in E^d increases rapidly with increasing dimension d. In dimensions 2 and 3 there exists only one combinatorial type of primitive parallelohedra. In $d = 2$ this is a hexagon and in $d = 3$ this is a truncated octahedron. In $d = 4$ there are three combinatorially different parallelohedra which are all principal primitive. In $d = 4$ there is also one non-primitive parallelohedron which has the same maximal number of faces as primitive ones. In dimension 5 as found by Engel [47], there are 222 combinatorially different types of primitive parallelohedra among which there are 21 non-principal. In dimension 6 only the lower bounds for the number of primitive parallelohedra are known [25]. There are at least 567613632 combinatorial types among which there are 293517383 non-principal ones.

  It is interesting to see the recently found results on the numbers N_k of k-faces of primitive parallelohedra [25]. They are reproduced in Table 6.2

TAB. 6.2 – The numbers N_k of k-faces of primitive parallelohedra in E^d, $2 \leq d \leq 6$. Different sets of numbers N_k of k-faces for six-dimensional non-primitive parallelohedra correspond to sixteen different values of $t = 1, 2, \ldots, 16$. The table is based on the numerical data given in [25].

d	N_0	N_1	N_2	N_3	N_4	N_5	Belts
2	6	6					6_1
3	24	36	14				6_6
4	120	240	150	30			6_{25}
5	720	1800	1560	540	62		6_{90}
	708	1770	1536	534	62		6_{89}
6	5040	15120	16800	8400	1806	126	6_{301}
	$5040 - 28t$	$15120 - 84t$	$16800 - 90t$	$8400 - 40t$	$1806 - 6t$	126	6_{301-t}

in a slightly different manner which explicitly shows that for non-principal primitive parallelohedra the $d + 1$ dimensional vector of numbers N_k, $k = 0, 1, \ldots, d$ can be written as a linear function of only one auxiliary parameter chosen in Table 6.2 as t and taking for $d = 5$ only one value $t = 1$ and for $d = 6$ taking 16 consecutive values $t = 1, \ldots, 16$.

The origin of this linear dependence on only one auxiliary parameter remains unexplained for non-principal primitive parallelohedra. Several linear relations between numbers of k-faces are known for a larger class of convex polytopes, namely for simple polytopes.

Definition: simple polytope A d-dimensional polytope P is called *simple* if every vertex v of P belongs to exactly d facets of P.

The class of simple polytopes is larger than the class of primitive polytopes defined in terms of primitive tilings. For example the d-dimensional cube is simple but not the primitive polytope. For a simple d-dimensional polytope the system of linear relations between numbers of k-faces (known as Dehn-Sommerville relations) consists of $\lfloor (d+1)/2 \rfloor$ relations, where $\lfloor x \rfloor$ is the integer part of x. The simplest way to introduce this relationship is to use the so called h-vectors of the polytope [2].

Definition: h-vector Let P be a d-dimensional simple polytope and $N_k(P)$ be the number of k-dimensional faces of P (we agree that $f_d(P) = 1$). Let

$$h_k(P) = \sum_{i=k}^{d} (-1)^{i-k} \binom{i}{k} N_i(P) \quad \text{for} \quad k = 0, \ldots, d. \qquad (6.51)$$

The $(d+1)$-tuple $(h_0(P), \ldots, h_d(P))$ is called the h-vector of P.

It can be proved that the numbers of k-faces, N_k, can be uniquely determined from $h_k(P)$:

$$N_i(P) = \sum_{k=i}^{d} \binom{k}{i} h_k(P) \quad \text{for} \quad i = 0, \ldots, d. \qquad (6.52)$$

Now we formulate without proof the following important proposition.

Proposition 33 (Dehn-Sommerville relations). *Let P be a simple d-dimensional polytope. Then*

$$h_k(P) = h_{d-k}(P) \quad \text{for} \quad k = 0, \ldots, d. \tag{6.53}$$

and

$$1 = h_0 \leq h_1 \leq \ldots \leq h_{\lfloor d/2 \rfloor}. \tag{6.54}$$

For centrally symmetric simple d-polytopes Stanley [18, 90] improved inequality (6.54), namely:

$$h_i - h_{i-1} \geq \binom{d}{i} - \binom{d}{i-1}, \quad \text{for} \quad i \leq \lfloor d/2 \rfloor. \tag{6.55}$$

For primitive parallelohedra we can apply Dehn-Sommerville relations together with the explicit expression (6.48) for the number of facets of primitive parallelohedra and the upper bound for the number of k-faces of primitive parallelohedra given by Voronoï (6.47). Also we take into account that the number of k-faces of primitive parallelohedra should be a multiple of $2(d - k + 1)$ for $k \leq n - 1$ (see proposition 29).

For $d = 2$ the only Dehn-Sommerville relation coincides with Euler characteristic of the polytope. Together with $N_1 = 6$ (6.48) this determines the unique vector of the numbers of faces $(N_1 = 6, N_0 = 6)$ for the primitive 2-dimensional polytopes.

For $d = 3$ the second Dehn-Sommerville relation appears which can be written in a form applicable for any $d \geq 3$,

$$dN_0(P) = 2N_1(P) \quad \text{for} \quad d \geq 3. \tag{6.56}$$

Applying two Dehn-Sommerville relations to three-dimensional simple polytopes we get for the numbers of faces expression

$$(N_0 = 2N_2 - 4, \quad N_1 = 3N_2 - 6, \quad N_2), \tag{6.57}$$

which includes one free parameter, N_2. For primitive 3d-polytope the number of facets is $N_2 = 14$ (6.48) and we get the unique possible set of numbers of faces for 3d-primitive parallelohedron: $(N_0 = 24, N_1 = 36, N_2 = 14)$.

The same two general linear Dehn-Sommerville relations exist for 4d-simple polytopes. This means that we can express the numbers of k-faces for four dimensional simple polytopes in terms of two free parameters, say N_3 and N_2:

$$(N_0 = N_2 - N_3, \quad N_1 = 2N_2 - 2N_3, \quad N_2, \quad N_3). \tag{6.58}$$

It follows that for primitive 4-polytopes after imposing $N_3 = 30$ and $N_2 = 150 - 6\alpha$, we get for the number of faces and for the components of h-vector the following expressions which depend on one free parameter α:

$$N_0 = 120 - 6\alpha, N_1 = 240 - 12\alpha, N_2 = 150 - 6\alpha, N_3 = 30, N_4 = 1; \tag{6.59}$$

$$h_0 = 1 = h_4, \quad h_1 = 26 = h_3, \quad h_2 = 66 - 6\alpha. \tag{6.60}$$

Applying relation (6.54) we get immediately that α can take only a small number of values, namely $\alpha = 0, 1, 2, 3, 4, 5, 6$. But among these values only $\alpha = 0$ and $\alpha = 5$ give the number of vertices divisible by 10 and among these two possible values only $\alpha = 0$ gives the number of edges divisible by 8. Consequently, we get that the only possible set of the numbers of faces for primitive four-dimensional parallelohedra is ($N_0 = 120$, $N_1 = 240$, $N_2 = 150$, $N_3 = 30$, $N_4 = 1$).

For five dimensional simple polytopes there are three Dehn-Sommerville linear relations.

$$N_0 - N_1 + N_2 - N_3 + N_4 - 2 = 0; \tag{6.61}$$
$$N_1 - 2N_2 + 3N_3 - 5N_4 + 10 = 0; \tag{6.62}$$
$$N_2 - 4N_3 + 10N_4 - 20 = 0. \tag{6.63}$$

For primitive parallelohedra $N_4 = 62$ and we can express N_{d-2} as $N_3 = 540 - 6\alpha$ taking into account that primitive parallelohedra have only six-fold belts (i.e. N_{d-2} should be divisible by 6). This allows us to express all numbers of faces in terms of one free parameter α and to explain the linear relation between numbers of faces for 5d-primitive parallelohedra with 90 and 89 belts given in Table 6.2. Namely we get

$$(N_0 = 720 - 12\alpha, \quad N_1 = 1800 - 30\alpha, \quad N_2 = 1560 - 24\alpha,$$
$$N_3 = 540 - 6\alpha, \quad N_4 = 62) \quad \text{with} \quad \alpha = 0, 1, \ldots. \tag{6.64}$$

This expression fits numerical results listed in Table 6.2, but the restriction of α to only two possible values $\alpha = 0, 1$ remains unexplained. The inequality (6.55) allows only to state that $0 \le \alpha \le 40$.

For six-dimensional simple polytopes there are again three linear Dehn-Sommerville relations. Together with $N_5 = 126$ this gives for six-dimensional primitive polytopes expressions for the number of faces depending on two free parameters.

$$N_5 = 126; \quad N_4 = 1806 - 6\alpha; \quad N_3 = 8400 - 8\beta;$$
$$N_2 = 16800 + 30\alpha - 24\beta; \quad N_1 = 15120 + 36\alpha - 24\beta;$$
$$N_0 = 5040 + 12\alpha - 8\beta. \tag{6.65}$$

We see that for any integer α, β the N_4 is divisible by 6, the N_3 is divisible by 8, the N_1 is divisible by 12. At the same time N_2 becomes a multiple of 10 only for $\beta = 5\gamma$, with $\gamma = 0, 1, 2, \ldots$. Replacing β by 5γ we get

$$N_5 = 126; \quad N_4 = 1806 - 6\alpha; \quad N_3 = 8400 - 40\gamma;$$
$$N_2 = 16800 + 30\alpha - 120\gamma; \quad N_1 = 15120 + 36\alpha - 120\gamma;$$
$$N_0 = 5040 + 12\alpha - 40\gamma. \tag{6.66}$$

But we still need to check that N_0 is divisible by 14. This is equivalent to the requirement for $(3\alpha - 10\gamma)$ to be a multiple of 7. This is possible only

for $\alpha = 0, \gamma = 0, 7, 14, \ldots$; $\alpha = 1, \gamma = 1, 8, 15, \ldots$; $\alpha = 2, \gamma = 2, 9, 16, \ldots$, etc. More generally we should have $\gamma - \alpha = 7k$.

Taking into account that for any set of two free parameters, α, γ, the numbers of faces cannot exceed their values for principal primitive parallelohedra we get general restrictions on possible values of free parameters $0 \leq 3\alpha \leq 10\gamma$. Together with the divisibility constraint $\gamma = \alpha + 7k$, with k being any integer, it follows that for $\gamma = 0$ the only possible value of the second parameter is $\alpha = 0$. Similarly, for $\gamma = 1$ we should have $\alpha = 1$ and for $\gamma = 2$, $\alpha = 2$. Only starting from $\gamma = 3$, several values of the second parameter are possible, in particular formal solutions are $(\gamma = 3, \alpha = 3)$ and $(\gamma = 3, \alpha = 10)$. Numerical results given by Baburin and Engel [25] correspond to face vectors with $\alpha = \gamma = 0, 1, \ldots, 16$. The fact that for six-dimensional primitive parallelohedra the whole observed set of face vectors can be described as only one-parameter family should be related to additional properties of primitive parallelohedra which are not taken into account in the present analysis.

It is clear that with increasing dimension the number of free parameters for the face vectors obtained within the adopted above scheme increases. For 7-dimensional parallelohedra we still have two free parameters but for 8-dimensional there are three such parameters, etc. The question whether the exact solution for face vectors of primitive parallelohedra in arbitrary dimension can be described by a one parameter family or a multi-parameter family is an interesting open problem.

6.4.1   Four dimensional lattices

This section illustrates correspondence between description of the four-dimensional lattices in terms of combinatorial types of parallelohedra and in terms of the subdivision of the cone of positive quadratic forms.

In four-dimensional space E^4 there exist three types of primitive parallelohedra which are principal (i.e. have the maximal numbers of k-faces for all k, namely $N_3 = 30, N_2 = 150, N_1 = 240, N_0 = 120$). Corresponding quadratic forms fill on the 10-dimensional cone of positive quadratic forms in four variables the 10-dimensional generic domains. Along with three primitive parallelohedra there exist one combinatorial type which is not primitive but has the maximal number of facets. The face vector for this non-primitive but maximal type is ($N_3 = 30, N_2 = 144, N_1 = 216, N_0 = 102$). The quadratic forms associated with this non-primitive parallelohedron form a 9-dimensional domain.

Starting from these four maximal parallelohedra all other combinatorial types can be obtained by a consecutive application of the zone contraction. There are two zone-contraction/extension families consisting in 35 and 17 combinatorial types respectively. These two families are shown in Figures 6.10 and 6.11. The whole list of different combinatorial types of 4-dimensional parallelohedra was given initially by Delone [41] who found 51 types and
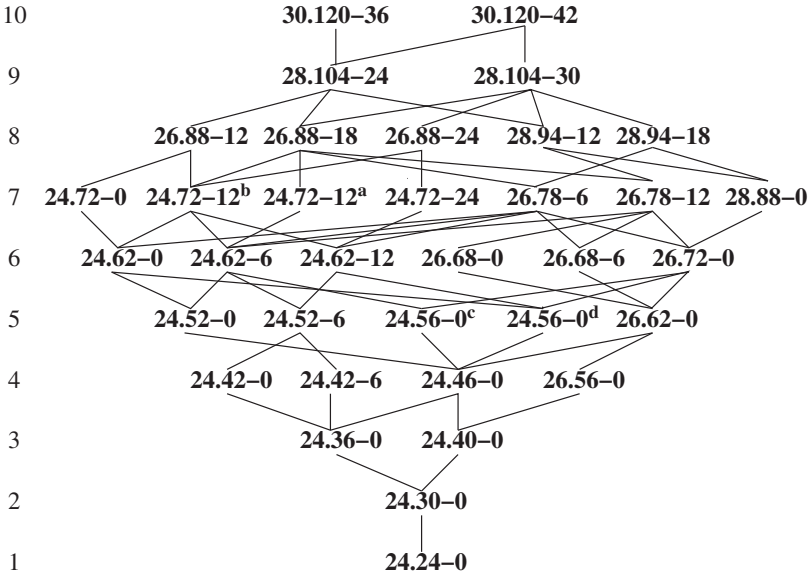
10		**30.120–36**		**30.120–42**		
9			**28.104–24**		**28.104–30**	
8		**26.88–12** **26.88–18** **26.88–24**		**28.94–12** **28.94–18**		
7	**24.72–0** **24.72–12**[b] **24.72–12**[a] **24.72–24**		**26.78–6** **26.78–12** **28.88–0**			
6	**24.62–0** **24.62–6** **24.62–12**	**26.68–0**	**26.68–6** **26.72–0**			
5	**24.52–0** **24.52–6** **24.56–0**[c] **24.56–0**[d] **26.62–0**					
4	**24.42–0** **24.42–6** **24.46–0** **26.56–0**					
3	**24.36–0** **24.40–0**					
2	**24.30–0**					
1	**24.24–0**					

FIG. 6.10 – Zone contraction/extension family of Voronoï cells in E^4 consisting of 35 combinatorial types including two primitive cells, **30.120**-42 and **30.120**-36 and **24.24**-0 cell (F_4). Each cell is denoted by a $\mathbf{N_3.N_0}$-n_6 symbol where n_6 is the number of hexagonal 2-faces. When this symbol is insufficient for a unique definition of the cell we give as a footnote the 3-subordination symbol: a - $8_{12}10_{12}$; b - $8_{14}10_812_2$; c - $8_{16}10_8$; d - $8_{18}10_412_2$. The dimension of the corresponding regions within the ten-dimensional cone of positive quadratic forms is indicated on the left. Note that some minor modifications have been introduced into the original figure taken from [11]. The modifications are justified by an explicit graphical correlation discussed in the next section.

was corrected by Shtogrin [87], adding one missed type. The organization of combinatorial types into two families was studied by Engel [11, 49]. (For a more detailed recent analysis see [32, 91, 44]. We will discuss briefly this organization using graphical representation in the next section 6.7.)

Each of the three primitive parallelohedra are associated with a 10-dimensional domain on the cone of the positive quadratic cone bounded each by 10 hyperplanes (walls). Schematic representation of these generic domains is given in Figure 6.12. (We return to the more profound discussion of this figure in section 6.8 after introducing graphical representation.) We use in these figures an abbreviated notation for primitive parallelohedra used by Engel [11], namely **30.120**-60 is denoted by "2"; **30.120**-42 is denoted by "3"; and **30.120**-36 is denoted by "4". All walls between **30.120**-60 and **30.120**-42 (i.e. between "2" and "3") are of **28**.**96**-40 type. It is important that the

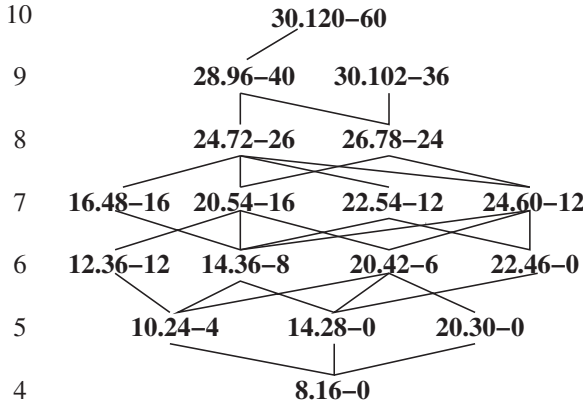|		
10		**30.120–60**
9	**28.96–40**	**30.102–36**
8	**24.72–26**	**26.78–24**
7	**16.48–16** **20.54–16**	**22.54–12** **24.60–12**
6	**12.36–12** **14.36–8**	**20.42–6** **22.46–0**
5	**10.24–4** **14.28–0**	**20.30–0**
4		**8.16–0**

FIG. 6.11 – Zonohedral contraction/extension family of Voronoï cells in E^4 consisting of 17 cells. Notation is explained in caption to figure 6.10. The dimension of the corresponding regions within the ten-dimensional cone of positive quadratic forms is indicated on the left.

passage from "2" to the **28.96**-40 wall corresponds to the contraction of the **30.120**-60 parallelohedron whereas there is no contraction/extension transformation between "3", i.e. **30.120**-42 and the same wall **28.96**-40. All walls between disconnected domains of "3" type (i.e. **30.120**-42) are of **28.104**-30 type. They correspond to contraction of the cell "3".

Each isolated domain of **30.120**-36 type (i.e. of type "4") has nine walls of **28.104**-24 type separating "4" and "3" and associated with contraction from both sides and one wall between two disconnected domains of the same type "4". This wall is of **30.102**-36 type. It corresponds to a non-primitive paralelohedron with maximal number of facets and there is no contraction leading from the region "4" to that wall.

Finally the domain "3" (i.e. **30.120**-42) has six walls with similar disconnected domains of the same type "3", three walls with domains of type "4" (i.e. **30.120**-36) and one wall with domain "2" (i.e. **30.120**-60).

6.5 Partition of the cone of positive-definite quadratic forms

We describe now in slightly more detail the algebraic structure of the cone of positive-definite quadratic forms in n variables. Special attention will be paid now to the evolution of combinatorial type along a path in the space of positive quadratic forms going from one generic domain to another different (or equivalent by $GL_n(\mathbb{Z})$ transformation) domain by crossing the wall.
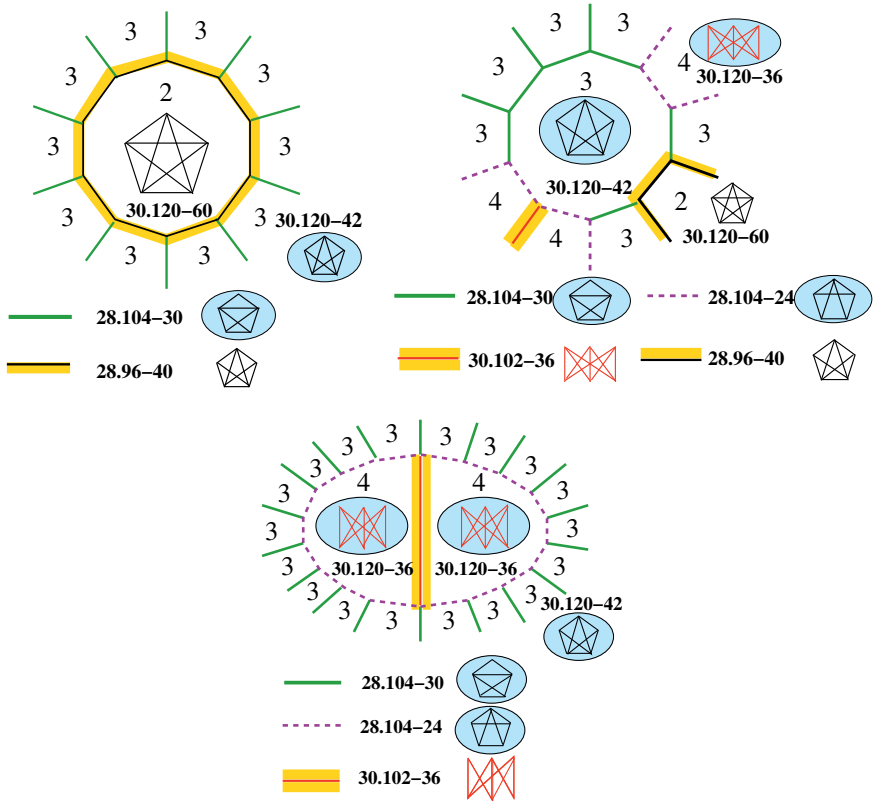
FIG. 6.12 – Schematic representation of local arrangements of generic subcones of the cone of quadratic forms for $d = 4$. Ten-dimensional domains with nine-dimensional boundaries are represented by two-dimensional regions with one-dimensional boundaries. **30.120**-36 type is abbreviated as "4", **30.120**-42 type as "3", and **30.120**-60 type as "2" in accordance with notation used by Engel [11]. For comments on graphical visualization see section 6.8.

A quadratic form is defined by $\varphi(\vec{x}) := \vec{x}^{t} Q \vec{x}$. We denote by

$$\mathcal{C}^{+} := \left\{ Q \in \mathbb{R}^{\binom{n+1}{2}} | \varphi(\vec{x}) > 0, \forall \vec{x} \in E^{n} \setminus \{0\} \right\} \qquad (6.67)$$

the cone of positive-definite quadratic forms. Its dimension is $\binom{n+1}{2} = \frac{n(n+1)}{2}$. The closure of the cone is denoted by $\mathcal{C} := clos(\mathcal{C})^{+}$, and its boundary by $\mathcal{C}^{0} := \mathcal{C} \setminus \mathcal{C}^{+}$.

Given an orthonormal basis $\vec{e}_{1}, \ldots, \vec{e}_{n}$ of $\mathbb{R}^{n}$, a basis of $\mathbb{R}^{n \times n}$ is obtained by the tensor products $\vec{e}_{ij} := \vec{e}_{i} \otimes \vec{e}_{j}$, $i, j = 1, \ldots, n$, with $\vec{e}_{ij} \vec{e}_{kl} = \delta_{ik} \delta_{jl}$. Since Q is symmetric, $Q = Q^{t}$, it follows that the cone $\mathcal{C}^{+}$ can be restricted to a subspace $\mathbb{R}^{\binom{n+1}{2}}$ of dimension $\binom{n+1}{2}$, defined by $\vec{e}_{ij} = \vec{e}_{ji}$, $i \leq j = 1, \ldots, n$.

In $\mathbb{R}^{n \times n}$, the Gram matrix Q is represented by a vector $\vec{q}$ with components q_{ij}, $1 \leq i, j \leq n$. Each zone vector $\vec{z}^*$ has a representation in $\mathbb{R}^{n \times n}$ by $\vec{z}^* \otimes \vec{z}^*$.

One can study the symmetry of a lattice L by investigating the symmetry of its Gram matrix in the cone $\mathcal{C}^+$. For any $A \in GL_n(\mathbb{Z})$, $Q' = AQA^{\mathrm{t}}$ is arithmetically equivalent to Q. Thus, $\vec{q}\,' = A^{\mathrm{t}} \otimes A^{\mathrm{t}}\vec{q}$ is arithmetically equivalent to q. If $S \in GL_n(\mathbb{Z})$ fixes Q, $Q = SQS^{\mathrm{t}}$, then $S^{\mathrm{t}} \otimes S^{\mathrm{t}}$ fixes $\vec{q}$.

For any vector $\vec{v}^* = v_1 \vec{a}_1^*, \ldots, v_n \vec{a}_n^*$ in dual space, the tensor product $\vec{l} = \vec{v}^* \otimes \vec{v}^*$ is denoted to be a ray vector. Since $\det(\vec{v}^* \otimes \vec{v}^*) = 0$, it follows that the ray vector $\vec{l}$ lies on the boundary $\mathcal{C}^0$. Let $\vec{c}$ be the representation of the identity matrix in $\mathbb{R}^{n \times n}$. Then $\lambda \vec{c}$ is the axis of the cone $\mathcal{C}$, because for any ray vector $\vec{l}$, the cone angle ψ satisfies

$$\cos \psi = \frac{\vec{c} \cdot \vec{l}}{|\vec{c}||\vec{l}|} == \frac{v_1^2 + v_2^2 + \ldots + v_n^2}{\sqrt{n}\sqrt{v_1^4 + 2v_1^2 v_2^2 + \ldots + v_n^4}} = \frac{1}{\sqrt{n}}. \tag{6.68}$$

Thus $\mathcal{C}$ is a cone of rotation with rotation axis $\lambda \vec{c}$. For $n = 2$ the cone angle ψ is $\pi/4$ (see Figure 6.1). For large dimensions n, the cone angle ψ is close to $\pi/2$. The cone $\mathcal{C}$ is intersected by subspaces of dimensions $\binom{k+1}{2}$, $k < n$.

Let us now study partition of the cone $\mathcal{C}$ into domains of non-equivalent combinatorial types.

Definition: domain of combinatorial type In the cone $\mathcal{C}$, the domain of combinatorial type of a parallelohedron P is the connected open subcone of Gram matrices

$$\Phi^+(P) = \{Q \in \mathcal{C}^+ | P(Q) \overset{\text{comb}}{\simeq} P\}. \tag{6.69}$$

By $\Phi = clos(\Phi^+)$ we denote its closure, and its boundary is given by $\Phi^0 = \Phi \setminus \Phi^+$.

Theorem 10 *The domain Φ of the combinatorial type of a parallelohedron P is a polyhedral subcone of $\mathcal{C}$.*

Proof. We have to show that the border between two neighboring domains of parallelohedra of different combinatorial type are flat walls. It is sufficient to do that for generic domains, the walls are then hyperplanes in $\mathcal{C}$. We give the condition for the existence of a wall $W \subset \Phi$. Let Φ be a generic domain. The length of at least one edge of P diminishes for some $Q \in \Phi^+$ approaching the boundary Φ^0, and when Q hits Φ^0, both vertices subordinated to that edge coincide. By this coincidence at least $n + 1$ facets meet in the common vertex v. If a facet F_i contains the vertex v then the corresponding facet vector $\vec{f}_i$ fulfills the equation

$$\vec{v}\,^{\mathrm{t}}Q\vec{f}_i = \frac{1}{2}\vec{f}_i\,^{\mathrm{t}}Q\vec{f}_i, \quad i = 1, \ldots, n + 1. \tag{6.70}$$

As a sufficient condition that $n + 1$ facets meet in the vertex v, we have that the determinant

$$
\begin{vmatrix}
\sum q_{1j} f_{1j} & \cdots & \sum q_{nj} f_{1j} & \vec{f}_1{}^t Q \vec{f}_1 \\
\cdot & & \cdot & \cdot \\
\cdot & & \cdot & \cdot \\
\cdot & & \cdot & \cdot \\
\sum q_{1j} f_{nj} & \cdots & \sum q_{nj} f_{nj} & \vec{f}_n{}^t Q \vec{f}_n \\
\sum q_{1j} f_{n+1,j} & \cdots & \sum q_{nj} f_{n+1,j} & \vec{f}_{n+1}^t Q \vec{f}_{n+1}
\end{vmatrix} = 0. \qquad (6.71)
$$

Since $\vec{f}_1, \ldots, \vec{f}_n$ form a basis of a sublattice of L of index ω, it follows that

$$
\vec{f}_{n+1} = \alpha_1 \vec{f}_1 + \ldots + \alpha_n \vec{f}_n, \quad \alpha_i, \in \mathbb{Z}/\omega\mathbb{Z}. \qquad (6.72)
$$

Hence, the determinant can be transformed to

$$
\begin{vmatrix}
\sum q_{1j} f_{1j} & \cdots & \sum q_{nj} f_{1j} & \vec{f}_1{}^t Q \vec{f}_1 \\
\cdot & & \cdot & \cdot \\
\cdot & & \cdot & \cdot \\
\cdot & & \cdot & \cdot \\
\sum q_{1j} f_{nj} & \cdots & \sum q_{nj} f_{nj} & \vec{f}_n{}^t Q \vec{f}_n \\
0 & \cdots & 0 & A
\end{vmatrix} = 0, \qquad (6.73)
$$

where

$$
A := \sum_{i=1}^{n} \alpha_i(\alpha_i - 1)\vec{f}_i{}^t Q \vec{f}_i + 2\sum_{i=1}^{n-1}\sum_{j=i+1}^{n} \alpha_i \alpha_j \vec{f}_i{}^t Q \vec{f}_j. \qquad (6.74)
$$

We set

$$
\Delta_n = \begin{vmatrix}
\sum q_{1j} f_{1j} & \cdots & \sum q_{nj} f_{1j} \\
\cdot & & \cdot \\
\cdot & & \cdot \\
\cdot & & \cdot \\
\sum q_{1j} f_{nj} & \cdots & \sum q_{nj} f_{nj}
\end{vmatrix}. \qquad (6.75)
$$

The determinant thus becomes

$$
A\Delta_n = A \, \det(Q) \, \det(\vec{f}_1, \ldots, \vec{f}_n) = 0. \qquad (6.76)
$$

This product gives, in terms of the Gram matrix Q, the condition that the $n + 1$ facets meet in the vertex v. Either factor can be zero.

- First consider the case $A = 0$. The term A is linear in the q_{ij} and hence, it determines a flat wall $W \subset \Phi$.
- The case $\det(Q) = 0$, or $\det(\vec{f}_1, \ldots, \vec{f}_n) = 0$ means that $Q \in \mathcal{C}^0$ and the lattice L^n degenerates to L^k, $k < n$.

The parallelohedron P has only a finite number of edges, and therefore Φ is bounded by a finite number of hyperplanes. Thus Φ is a rational polyhedral subcone of $\mathcal{C}$.   □

Since ω is finite, the term A can be represented by integral numbers h_{ij}, and thus the coincidence condition becomes

$$h_{11}q_{11} + h_{12}q_{12} + \ldots + h_{nn}q_{nn} = 0. \tag{6.77}$$

The wall normal

$$\vec{n} = h_{11}\vec{e}_{11} + h_{12}\vec{e}_{12} + \ldots + h_{nn}\vec{e}_{nn} \tag{6.78}$$

is orthogonal to the wall W.

In general, the wall W separates two domains of different combinatorial type. The wall itself is an open domain $\overline{\Phi}^+$ for some limiting type.

The edges of Φ are the extreme forms of Φ, and are referred to as edge forms. An edge form is either

- a ray vector lying on the boundary $\mathcal{C}^0$ which has a representation as a tensor product $\vec{z}^* \otimes \vec{z}^*$ with zero determinant, where $\vec{z}^*$ is a vector of a closed zone of P.
- a generic inner edge form of $\mathcal{C}^+$ having positive determinant.
- a non-generic inner edge form of $\mathcal{C}^+$ having zero determinant, i.e. it is a generic inner edge form of a cone $\overline{\mathcal{C}}^+$ of a lower dimension $\binom{k+1}{2}$, $k < n$. Inner edge forms occur only in dimensions $n \geq 4$.

An effective numerical algorithm to determine the walls and the edge forms is discussed in [25].

6.6   Zonotopes and zonohedral families of parallelohedra

After looking at the system of different combinatorial types of parallelohedra and their organization in families for four-dimensional lattices we return to some systematic classification of combinatorial types of parallelohedra for arbitrary dimension. We start with the definition of the Minkowski sum of polytopes.

Definition: Minkowski sum The vector sum or Minkowski sum of two convex polytopes P and P' is the polytope

$$P + P' = \{x + x' | x \in P, x' \in P'\}. \tag{6.79}$$

Equivalently, we can describe $P + P'$ as the convex sum of all combinations of their vertices. Let $V(P)$ and $V(P')$ be the set of vertices of P and P', then

$$P + P' = \text{conv}\{v + v' | v \in V(P), v' \in V(P')\}. \tag{6.80}$$

This can be generalized to any finite number of summands in an obvious way.

Now we define one special but very important class of polytopes.

Definition: Zonotope A zonotope is a finite vector sum of straight line segments.

We recall that a zone Z of a parallelohedron P is the set of all 1-faces (edges) E that are parallel to a zone vector $\vec{z}^*$,

$$Z := \{E \subset P | E \| \vec{z}^*\}. \tag{6.81}$$

In each edge at least $d - 1$ facets meet. The zone vector $\vec{z}^*$ is the outer product of the corresponding facet vectors. In the dual basis, $\vec{z}^*$ has integer components

$$\vec{z}^* = z_1 \vec{a}_1^* + \ldots + z_n \vec{a}_n^*, \quad z_i \in \mathbb{Z}. \tag{6.82}$$

With respect to any zone vector $\vec{z}^*$ we can classify the lattice vectors in layers

$$L_i(\vec{z}^*) := \{\vec{t} \in L^n | \vec{t}\vec{z}^* = i, \quad |i| = 0, 1, \ldots\}. \tag{6.83}$$

A zone Z is referred to as being closed if every 2-face of P contains either two edges of Z, or else none. Otherwise Z is denoted as being open.

The zone contraction is the process of contracting every edge of a closed zone by the amount of its shortest edges. As a result, the zone becomes open, or vanishes completely, but the properties of a parallelohedron are maintained and the result of the zone contraction is a parallelohedron of a new combinatorial type. If a d-dimensional parallelohedron P collapses under a zone contraction, then the resulting P' parallelohedron has dimension $d - 1$.

A parallelohedron P_c is referred to as being totally contracted, if all its zones are open. It is relatively contracted, if each further contraction leads to a collapse into a parallelohedron of a lower dimension. A parallelohedron P_m is maximal, if it cannot be obtained by a zone contraction of any other parallelohedron in the same dimension.

Note that a polytope P is a zonotope if and only if all its k-faces are centro-symmetric. In its turn, a zonotope is a parallelohedron if and only if all its belts have 4 or 6 facets. This is a consequence of Theorem 5.

The parallelohedra which are at the same time zonotopes have a particular simple combinatorial structure. They are named zonohedral parallelohedra.

For zonohedral parallelohedra P the following two conditions are equivalent:

i) each zone of P has edges of the same length;
ii) each zone of P is closed.

In each dimension there exists a unique family of parallelohedra which contains all zonohedral parallelohedra, and which is named a zonohedral family. In dimensions $d \leq 3$ all parallelohedra are zonohedral and belong to the

unique family. The zonohedral family for $d = 4$ consists of 17 members shown in Figure 6.11.

In dimensions $d \geq 4$ the zonohedral family includes several maximal zonotopes. For $d = 4$ (see figure 6.11), for example, the zonotopes $\mathbf{30.120 - 60}$ and $\mathbf{30.102 - 36}$ are maximal. Each zonohedral family has one main zone-contraction lattice corresponding to the maximal zonohedral parallelohedron $P_m(\mathbf{A}_n^*)$ of the root lattice $\mathbf{A}_n^*$ which is a primitive principal and generic, i.e. fills $d(d + 1)/2$-dimensional domain of the cone of positive quadratic forms. This main zone-contraction sub-family of the zonohedral family includes all parallelohedra which can be obtained from the $P_m(\mathbf{A}_n^*)$ zonotope by zone contraction. For dimension 4 (see again Figure 6.11) the main zone contraction sub-family consists of all zonotopes except one, namely $\mathbf{30.102 - 36}$. One contraction is necessary to transform $\mathbf{30.102 - 36}$ to a parallelohedron belonging to the main zone-contraction sub-family. Each maximal zonotope can be characterized by the number of zone-contraction steps needed to attain the main zone-contraction family. In dimension $d = 4$, the $\mathbf{30.102 - 36}$ parallelohedron is distanced from the main zone-contraction family by one step (contraction till $\mathbf{26.78 - 24}$). The zonohedral family for $d = 5$, for example, includes 81 zonotopes (see section 6.7), among which there are four maximal, with the maximal distance from main zone-contraction sub-family consisting of three contraction steps.

The minimal member of the zonohedral family has combinatorial type of a parallelepiped (hypercube) and occupies a d-dimensional domain on the cone of positive quadratic forms.

Apart from the zonohedral family in each dimension $d \geq 4$ there exist a number of parallelohedra which can be represented as a finite Minkowski sum of a totally zone contracted parallelohedron and a zonotope [51]. In dimension $d = 4$ the family consisting of 35 parallelohedra (see figure 6.10) can be constructed by applying a zone extension operation to the totally contracted 24-cell parallelohedron $\mathbf{24.24 - 0}$ associated with F_4 lattice.

Not every totally contracted parallelohedron can be extended by applying a Minkowski sum with a segment (without extending the dimension of the parallelohedron). The maximal and simultaneously totally contracted parallelohedron, for example, exists in $d = 6$. It is related to the E_6^* lattice [50, 57].

6.7 Graphical visualization of members of the zonohedral family

The fact that all members of the zonohedral family can be represented as a vector sum of a certain number of segments (vectors) allows us to construct relatively simple visualization of different combinatorial types of zonohedral lattices using graphs in such a way that each segment generating the
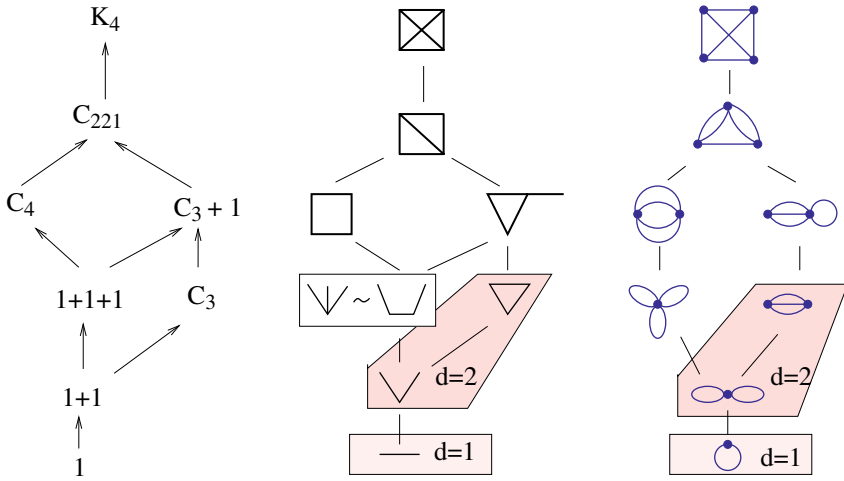
FIG. 6.13 – Graphical (center) and cographical (right) representations of zonohedral parallelotopes in dimensions $d = 1, 2, 3$ together with zone extension relations between them. The left diagram gives the notation of graphs used for graphical representation, as introduced in [32].

Minkowski sum is represented by a segment whereas linear dependencies between vectors corresponds to cycles of the graph. We cannot enter here into detailed mathematical theory of such a correspondence which is based on the matroid theory (for introduction see [23]). We hope that the more or less self-explaining correspondence shown in Figure 6.13 for dimensions $d = 1, 2, 3$ and in further figures for dimension $d = 4$ and $d = 5$ will stimulate the interest of the reader to study the corresponding mathematical theory.

The so called graphical representation for d-dimensional zonotopes consists in constructing connected graphs with $d+1$ nodes without loops and multiple edges. For $d = 1$ we obviously have one graph, for $d = 2$ there are two graphs (see Figure 6.13, center). In dimension $d = 3$ we need to introduce the equivalence relation between graphs, namely, for edges with one free end we should allow the other end of the same edge to move freely from one node to another. This means that all "tree-like" graphs or subgraphs should be treated as equivalent (see the equivalence between two three-edge graphs for $d = 3$ in Figure 6.13, center). This gives five inequivalent graphs for $d = 3$. For the notation of graphs (see left subfigure in 6.13) we follow the style used in the book [23].[9] The most important for further applications is the notation

---

[9] In [35], Conway and Sloane use these five graphs among different alternative versions of graphical visualizations and indicate as inconvenience the absence of symmetry transformations for this presentation. We note, however, that looking at these graphs up to topological equivalence, including 2-isomorphism [97] removes this inconvenience.

K_4 and its natural generalization to K_{d+1}, $d \geq 3$, which means the complete graph on four (or more generally on $d+1$) nodes. For dimension three, all five combinatorial types correspond exactly to all five connected graphs on four nodes (taking into account the introduced equivalence of graphs).

It is easy to see that the correlation between graphs (shown by connecting lines) corresponds to removing or adding one edge, when this correlation is within different graphs of the same number of nodes, i.e. between zonotopes of the same dimension. Removing one edge corresponds to zone contraction and all subgraphs of K_4 with four nodes can be obtained from K_4 by successively removing edges. Removing an edge with a free end leads to a graph with a lower number of nodes, i.e. we go to lower dimension with such a transformation.

Along with the graphical representation for 1-,2-,-3-dimensional zonotopes we can equally use so called cographical representation which consists of replacing the graphical representation by a dual graph. To construct a dual graph, the original graph should be planar, i.e. when drawing a graph on paper (plane) no intersection or touching points between edges are allowed (except at the nodes). All graphs in Figure 6.13 are planar. (It is sufficient to deform graph K_4 to avoid the intersection of two edges.) To construct for a planar graph the dual graph, we need to associate with one connected domain of the plane a node and with each edge of the original graph an edge of the dual graph crossing this edge and relating nodes associated with left and right domains separated by an edge. (It may occur that the domain is the same and we get a loop.) The following simple examples give an intuitive understanding of the construction of the dual graph.
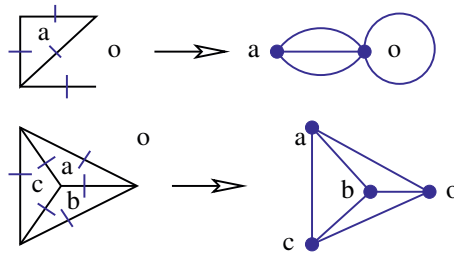
We see that a loop at one node and multiple edges between pairs of nodes appear naturally for a dual graph. Also we see that K_4 is self-dual. Elimination of one edge for graphical representation corresponds to shrinking of one edge by identifying two nodes for the corresponding dual graph. Increasing dimension for the graphical representation by adding one edge with a free end (adding an extra node) corresponds to adding a loop in the cographical representation. A cographical representation for three dimensional combinatorial types of lattices is given in Figure 6.13, right.

A very interesting and new situation (as compared with the three-dimensional case) appears for 4-dimensional zonotopes.
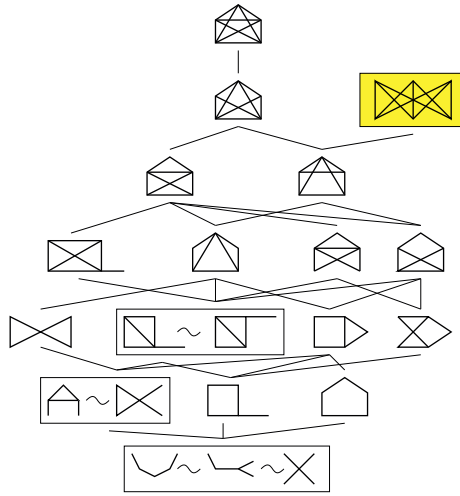
FIG. 6.14 – Zonohedral family in $d = 4$. A graphical representation is used for all zonohedral lattices except for the $K_{3,3}$ one. The arrangement of zonotopes reproduces the zonohedral family of lattices given in Figure 6.11.

Let us extend our visualization approach to the 4-dimensional case. Figure 6.14 gives a graphical representation for all zonohedral lattices for $d = 4$ (with exception of one case corresponding to maximal non-primitive **30.102**-36). In fact it is sufficient to construct all connected subgraphs of the complete graph K_5 with 5 vertices possessing 10 edges and to take into account certain equivalence relations. (The notations of graphs are summarized in Figure 6.15.) Certain equivalence relations in the graphical representation are shown in Figure 6.14. Namely, for C_3+1+1 and for $C_{2,2,1}+1$ graphs the edge with one free end can be attached to any node. To keep the figure more condensed we do not show for $C_3 + 1 + 1$ graph the isomorphism with the graph formed by a chain of length 2 attached to a 3-cycle. Starting from the complete graph K_5 we easily construct the zonohedral family consisting of 16 elements (except $K_{3,3}$ shown in Figure 6.14 in the special rectangle). To understand the logic of its appearance we need to study along with the graphical representation and the cographical one. First let us note that the K_5 graph is not planar and we cannot construct a dual for this graph. At the same time for all proper subgraphs of K_5 the dual graphs can be constructed. Figure 6.16 shows the result of cographical representations for all proper subgraphs of K_5. But this family naturally includes one extra graph, $K_{3,3}$ which can be obtained by an extension (point splitting) operation applied to the $K_5 - 1 - 1$ cographical representation. Point splitting is an inverse operation to edge contraction for the cographical representation. It allows us to find an
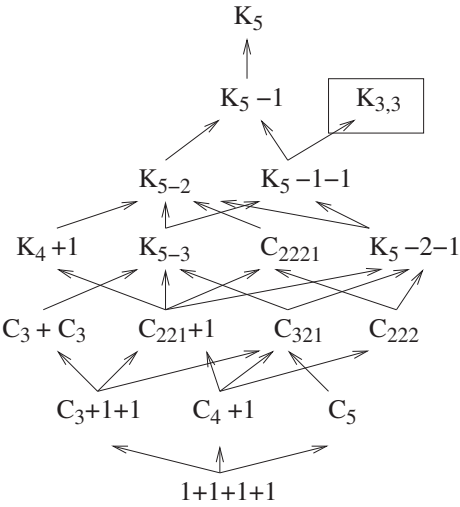
K_5

$K_5 - 1$ $\boxed{K_{3,3}}$

K_{5-2} $K_5 - 1 - 1$

$K_4 + 1$ K_{5-3} C_{2221} $K_5 - 2 - 1$

$C_3 + C_3$ $C_{221} + 1$ C_{321} C_{222}

$C_3 + 1 + 1$ $C_4 + 1$ C_5

$1 + 1 + 1 + 1$

FIG. 6.15 – Conway notation [32] for zonohedral family in $d = 4$. (Note the misprints in [32]: K_4 used by Conway should be replaced by $C_{221} + 1$, whereas K_4 corresponds to the primitive combinatorial type of the three-dimensional lattice.)
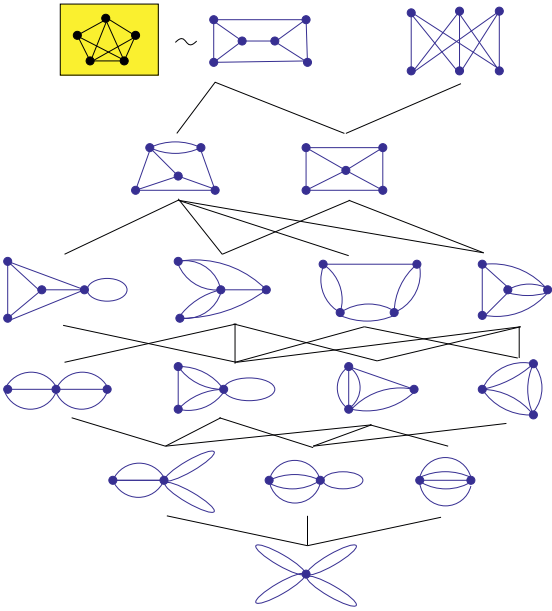

FIG. 6.16 – Cographical representation for 4-dimensional zonotopes.

additional zonotope belonging to a zonohedral family for four-dimensional lattices. Returning now to the semi-ordered set of zonotopes shown in Figure 6.14 we can explain the correlation between $K_5 - 1 - 1$ and $K_{3,3}$ as follows. From the graphical representation of $K_5 - 1 - 1$ we pass to the cographical representation and next realize point splitting of the only four-valence vertex. As a result we have two answers (depending on the type of rearrangement of edges during the point splitting), one is dual to $K_5 - 1$, another is $K_{3,3}$, for which we only have a cographical representation. These transformation are graphically summarized in the following symbolic equation.
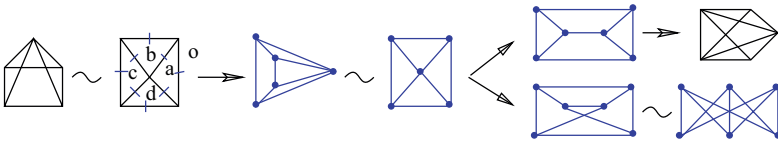
We use the four-dimensional case to introduce still one more representation of graphical zonotopal lattices. Namely, instead of plotting the graph which is a subgraph of K_5, we can simply plot the complement, i.e. the difference between K_5 and the subgraph. The only useful convention now is to keep all nodes explicitly shown. Such a representation is given in Figure 6.17. This representation becomes interesting when studying subgraphs with a number of edges close to the maximal possible value, i.e for subgraphs close to a complete graph K_5 and in higher dimensional cases close to K_{d+1}, or in other words for
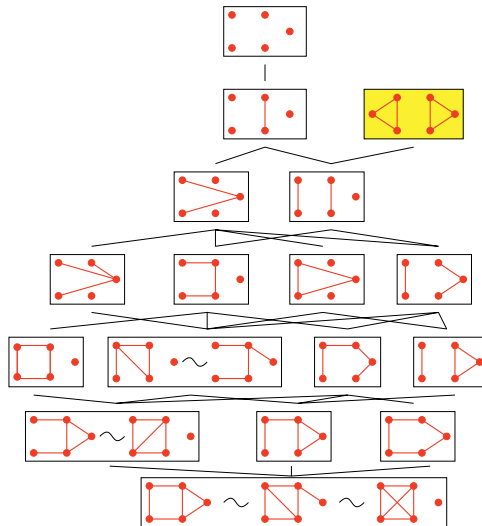

FIG. 6.17 – Representation of zonotopes through complement to graphical representation within the complete K_5 graph.

graphs with a small number of edges absent from the complete graph. This representation allows us to easily find equivalence between different graphical representations taking into account the topological equivalence of a complement to a graph. In contrast, for graphs with a small number of edges it is easier to see equivalence by looking directly at the graphical representation.

The five dimensional zonohedral family

To show the interest in the application of graphical visualization of zonohedral lattices we give now the application to five-dimensional lattices. The zonohedral family of five-dimensional lattices has been described by Engel [53], who has found 81 members of the family among which eight do not belong to the principal sub-family corresponding to the complete graph K_6 and its subgraphs. Engel characterizes members of the zonohedral family by symbols $N_{facets}.N_{vertices} - N_{hexagonal\ 2-faces}$ and gives the correlation between them corresponding to zone contraction. Figure 6.18 reproduces Engel's diagram with additional distinction between zonotopes belonging to
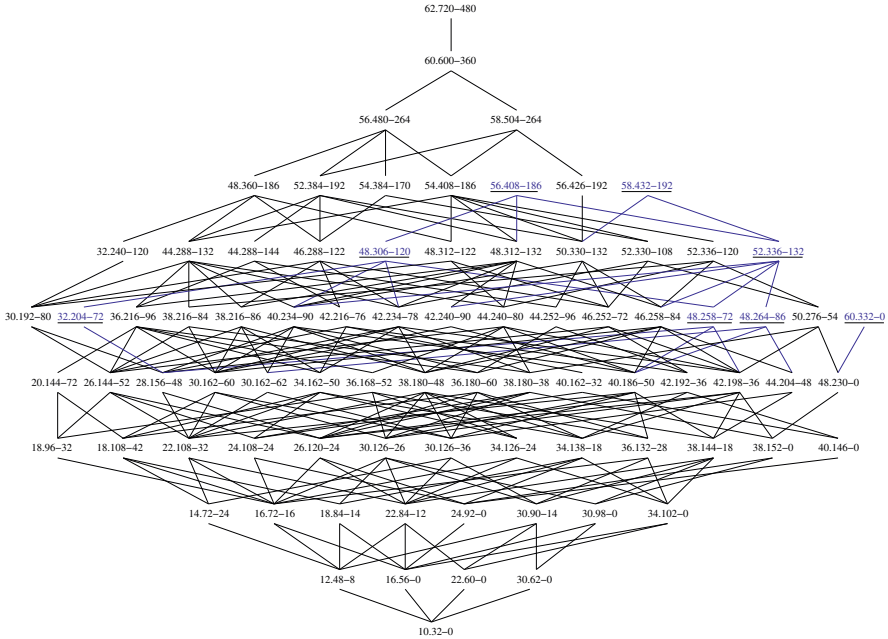

FIG. 6.18 – A representation of a zonohedral family in five-dimensional space made by Engel [53]. Lattices for which graphical representation is not available are underlined.

the main K_6-subfamily and correlations between members of this subfamily and zonotopes for which graphical representation is not available. Note that for the five-dimensional zonohedral lattices there exists one example of a lattice, namely **60.332**-0, which has neigher graphical nor cographical representation.

Figure 6.19 keeps the same organization of zonohedral lattices as that shown in Figure 6.18 but now each graphical lattice is given by its graph. Eight zonotopes which do not belong to the main family of subgraphs of K_6 are described by cographical representation or do not possess neigher graphical nor cographical representations. Their symbols are replaced in Figure 6.19 by an shaded rectangle. These lattices and their correlations with graphical lattices are discussed separately below.

To simplify the visualization for graphical representations we use graphs only when the number of edges is less than or equal to 10, whereas for graphs with the number of edges being more than or equal to 10 we use the representation of a complement to the graph with respect to the K_6 complete graph. For graphs with 10 edges both direct graphical and complement to graphical representations are given to clarify the correspondence.
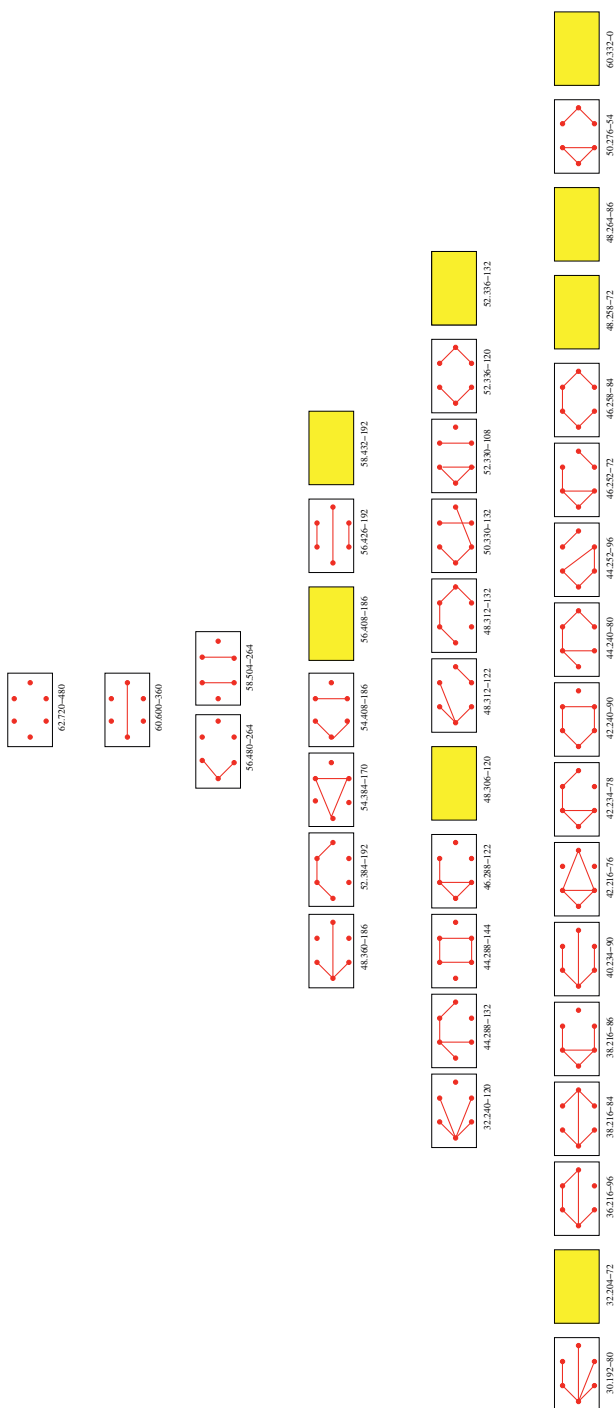
Let us now give some comments about zonohedral lattices which do not appear as subgraphs of the complete graph K_6. First consider **60.332**-0, which is a special R_{10} graph introduced by Seymour [86], or E_5 used by Danilov and Grishukhin [38]. This graph cannot be described as belonging to the graphical or cographical representations. It can be considered as an extension of the $K_{3,3}$ cographical four-dimensional lattice by adding one loop. Seymour [86] uses for R_{10} the presentation of the type
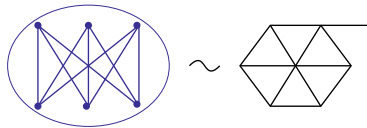
Note that the graphical presentation of **48.230**-0 as a subgraph of K_6 (which in fact equivalent as a graph to the $K_{3,3}$ representation) assumes that this graph corresponds to a five-dimensional lattice rather than the graph $K_{3,3}$ considered earlier and representing a four-dimensional zonohedral lattice. Because of that it is more natural to use $K_{3,3}^*$ notation for the four-dimensional lattice **30.120** $- 30$.

Let us now turn to cographical representation of seven zonohedral lattices which are not subgraphs of K_6. These seven cographical lattices are shown in Figure 6.20.

Figure 6.21 demonstrates using the example of the **58**.**432**-192 polytope how to realize different contractions. It is possible to make two contractions for **58**.**432**-192. One consists in the contracting edge between nodes 1 and 2. (Numbering is given in figure 6.21.) It leads to cographical representation of the **52.336**-132 polytope. Another contraction (15) leads to cographical

62.720-480

60.600-360

58.504-264

56.480-264

58.432-192

56.426-192

56.408-186

54.408-186

54.384-170

52.384-192

48.360-186

32.240-120

44.288-132

44.288-144

46.288-122

48.306-120

48.312-122

48.312-132

50.330-132

52.330-108

52.336-120

52.336-132

60.332-0

50.276-54

48.264-86

48.258-72

46.258-84

46.252-72

44.252-96

44.240-80

42.240-90

42.234-78

42.216-76

40.234-90

38.216-86

38.216-84
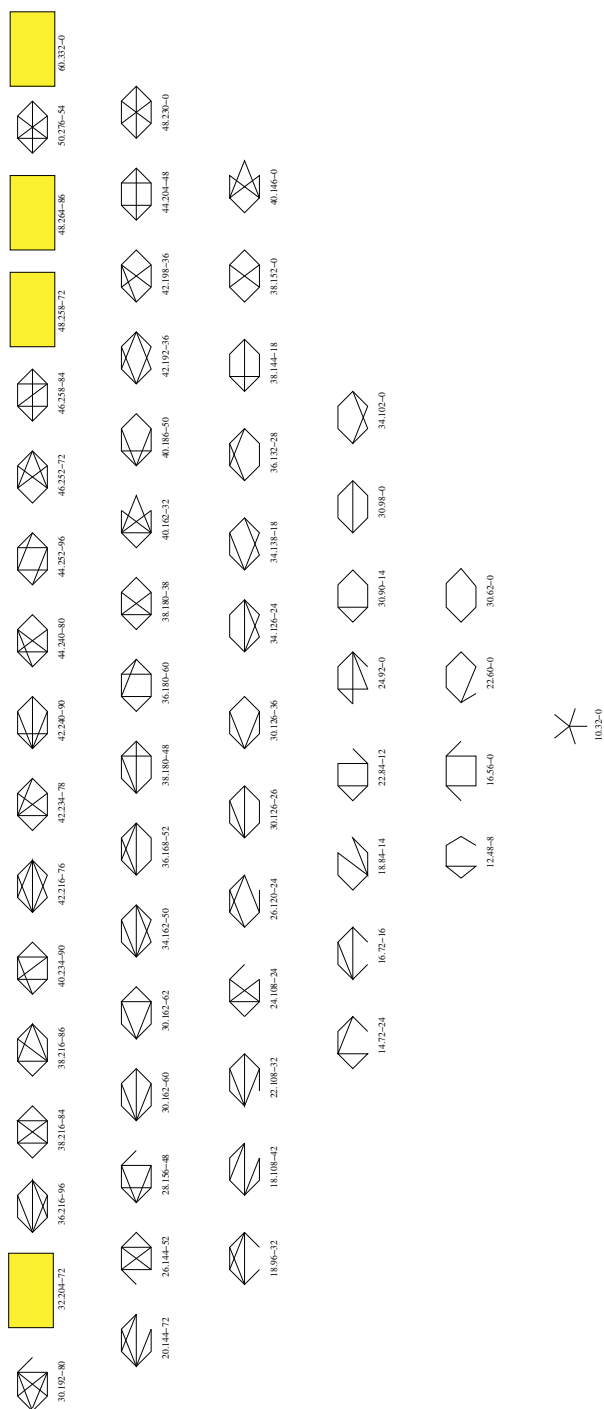
36.216-96

32.204-72

30.192-80

Fig. 6.19 – A representation of zonohedral family for five-dimensional lattices. For graphs with no more than 10 edges the direct representation is used, whereas complement graphs are drawn for graphs with 10 and more edges. Both direct and complement representations are shown for graphs with 10 edges in order to simplify the comparison between both representations. Graphs which are not subgraphs of K_6 are not shown in this figure. They are discussed separately. Their places in the original diagram by Engel are left free (shaded rectangle).
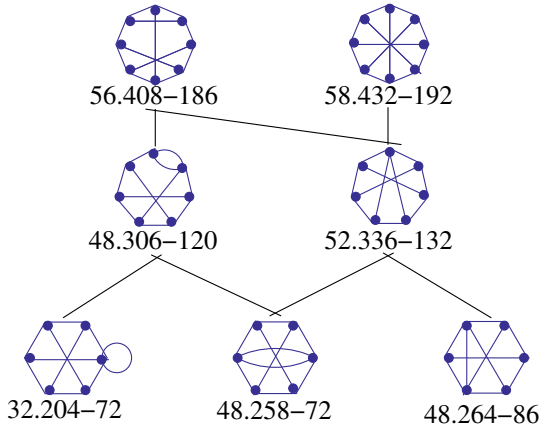
FIG. 6.20 – A cographical representation for seven zonohedral lattices associated with two maximal ones, **56.408**-186 and **58.432**-192. They are not shown in Figure 6.19.
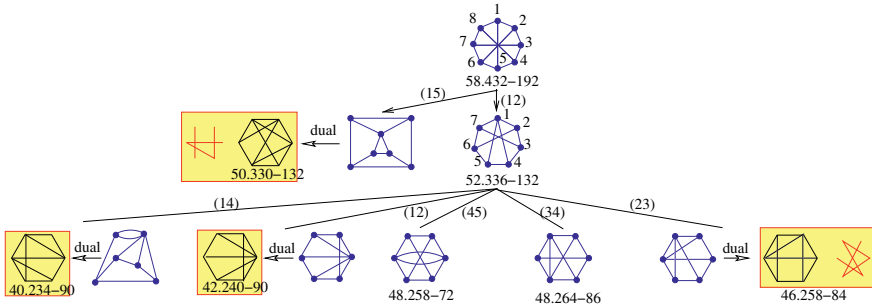

FIG. 6.21 – Different contractions of the **58.432**-192 zonohedral polytope shown in the cographical representation and transformed into the graphical representation for subgraphs of K_6.

representation which can be transformed to a dual graphical representation showing that the result is the polytope **50.330**-132. The complementary graph is given for **50.330**-132 along with the image of the graph itself in order to simplify the identification of the graph.

In its turn the cographical representation of the **52.336**-132 polytope shows that five different contractions are possible. Two among these contractions, namely (34) and (45) lead to two lattice zonotopes possessing only cographical presentation. Three other contractions (14), (12), and (23) lead to cographical presentation of zonotopes possessing graphical presentation

and being subgraphs of K_6. Their transformation to graphical presentation through construction of a dual graph is explicitly shown in Figure 6.21.

Graphical representation of subgraphs of K_6 gives us an opportunity to see explicitly an application of important notion of 2-isomorphism of graphs introduced by Whitney [97]. Namely, for the **30.162**-60 zonotope two apparently different graphs can be assigned, but nevertheless these two graphs are 2-isomorphic as the following graphical equation demonstrates.

6.7.1 From Whitney numbers for graphs to face numbers for zonotopes

Simple visualization of zonohedral lattices by graphs would be much more interesting if it is possible to find zonotopes characteristics directly form graphs. And this is indeed possible. Face numbers of zonotopes can be expressed through rather elementary formulae in terms of topological invariants of graphs, the so called Whitney numbers [96, 82, 56]. A short guide to the calculation of Whitney numbers for simple graphs is given in appendix B. Here we simply give several explicit expressions for face numbers of 3- and 4-dimensional zonotopes in terms of doubly indexed Whitney numbers of the first and second kind.

For three dimensional zonotopes, i.e. for all combinatorial types of three-dimensional lattices we have

$$N_0 = w_{00}^+ + w_{01}^+ + w_{02}^+ + w_{03}^+; \tag{6.84}$$
$$N_1 = w_{11}^+ + w_{12}^+ + w_{13}^+; \tag{6.85}$$
$$N_2 = w_{22}^+ + w_{23}^+; \tag{6.86}$$
$$N_2^{(6)} = 4w_{02}^+ - 2w_{12}^+; \tag{6.87}$$
$$N_2^{(4)} = 4w_{12}^+ - 6w_{02}^+. \tag{6.88}$$

where w_{ij}^+ are absolute value of doubly indexed Whitney numbers of the first kind.

In fact, the total number of k-faces can be expressed more generally for arbitrary dimension d as [56]

$$N_k = \sum_{j=k}^{d} w_{kj}^+. \tag{6.89}$$

For four-dimensional zonotopes we add several expressions for particular types of k-faces.

$$N_2^{(6)} = 2w_{13} + 4w_{23} + 2W_{13};$$

$$N_2^{(4)} = -2w_{13} - 6w_{23} - 2W_{13};$$

$$N_3^{(6)} = 2w_{01}w_{02} + 12w_{02} - 56w_{03} + 4w_{12} - 32w_{13} - 24w_{23} - 8W_{13};$$

$$N_3^{(8)} = -4w_{01}w_{02} - 24w_{02} + 96w_{03} - 8w_{12} + 50w_{13} + 36w_{23} + 14W_{13};$$

$$N_3^{(12)} = 4w_{01}w_{02} + 24w_{02} - 78w_{03} + 8w_{12} - 36w_{13} - 24w_{23} - 10W_{13};$$

$$N_3^{(14)} = -2w_{01}w_{02} - 12w_{02} + 36w_{03} - 4w_{12} + 16w_{13} + 10w_{23} + 4W_{13}.$$

Although these expressions are slightly complicated because they include one quadratic term, the existence of such expressions clearly supports the tight relation between zonohedral lattice and representative graph.

6.8 Graphical visualization of non-zonohedral lattices.

We have noted earlier in section 6.4.1, that in dimension four there exist two families of parallelohedra, the zonohedral family and the family obtained from the 24-cell polytope by making zone extension. This 24-cell family was represented in figure 6.10 taken (with minor modifications) from Engel's book [11]. In spite of the fact that these two families are often considered as completely independent and not related, there is a tight relation between them. The origin of this relation is the fact that all members of the 24-cell family can be constructed as a Minkowski sum of the 24-cell, $P_{24} = \mathbf{24.24}$-0 and a zonotope which we denote $Z(U)$ and which in its turn can be constructed as a Minkowski sum of one, two, three, or four vectors. Thus, we can try to associate with each non-zonohedral polytope a zonotope (one-, two-, three-, or four-dimensional) which after making a Minkowski sum with the 24-cell leads to a required polytope. We need however to mention here a very important remark made by Deza and Grishukhin [44]. For a zonotope $Z(U)$ itself it is not important whether the summing vectors are orthogonal or not. A parallelepiped and a cube have the same combinatorial type. But the orthogonality of summing vectors in $Z(U)$ influences heavily the combinatorial type of the sum $P_{24} + Z(U)$. This means that the number of different types of $P_{24} + Z(U)$ can be larger than the number of different $Z(U)$ and we need to introduce an additional index characterizing orthogonality or non-orthogonality of vectors in the sum associated with a zonotope $Z(U)$. Nevertheless the contraction/extension relation between different non-zonohedral polytopes should respect the corresponding contraction/extension relation between zonotopal contributions. This allows us to represent all non-zonohedral polytopes (or lattices) in a way similar to zonohedral ones. Figure 6.22 is a graphical
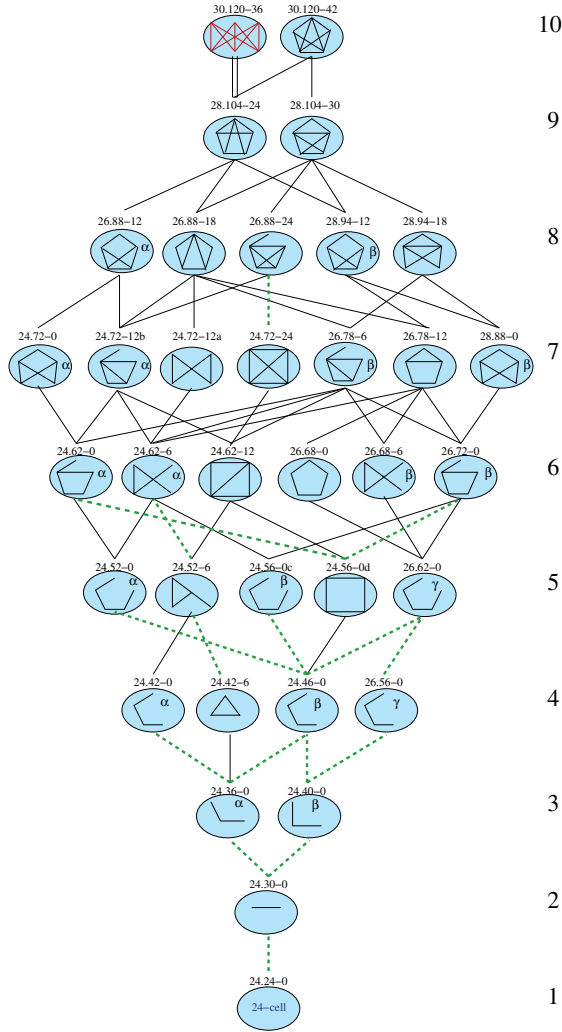
FIG. 6.22 – Graphical visualization of four-dimensional parallelohedra represented as a Minkowski sum $P_{24} + Z(U)$ of a zonotope $Z(U)$ and the 24-cell, $P_{24} = \mathbf{24.24} - 0$. Shaded elliptic disks symbolize the P_{24} cell. Graphs for zonotopes coincide with those used to visualize zonohedral lattices. Symbols α, β, γ make further distinction between zonotope contributions $Z(U)$. Depending on the number of mutually orthogonal vectors in the Minkowski sum for a zonotope $Z(U)$, this additional index characterizes the cases with no orthogonal edges, with a pair of orthogonal edges and with three mutually orthogonal edges. A single thin line corresponds to elimination/addition of one edge without changing the number of points. A double thin line symbolizes transformation to the dual representation. A thick dash line corresponds to elimination of one edge together with one point.

visualization of the organization of the 24-cell family shown in 6.10. In Figure 6.22 the 24-cell contribution to the sum is symbolized by an elliptic shaded disk. The zonotope contribution is represented inside the shaded disk in a way similar to the representation of zonotopes discussed in the preceding subsection. The additional index is added when it is necessary to distinguish between the Minkowski sum with the same zonotope contribution but with special orthogonality between vectors forming the zonotope. This additional index is shown on the disk and takes values α, β, γ. It is useful equally to make the distinction between correlations (contraction/extension) associated with elimination of one edge without changing the number of points, i.e. within the zonotopes of the same dimension, and with elimination of the edge together with one point. The correlations associated with modification of the dimension of a zonotope are represented by a thick dash line. Graphical correlation allows us to localize small misprints in the figure representing a partially ordered set of non-zonohedral lattices in book [11], Figure 9-7. Namely, in the notation used in [11] it is necessary to change the line 26-7$-$24-14 by the line 26-7$-$26-3; the line 26-6$-$26-3 should be changed into 26-6$-$24-14; the line 28-2$-$26-7 should be changed into 28-2$-$26-6.

Using the discussed above graphical visualization of non-zonohedral lattices we can better understand the system of the organization of walls between generic domains for a cone of positive quadratic forms (see figure 6.12). The wall between the 30-2 and 30-3 domains is of **28.96**-40 type represented by $(K_5 - \mathbf{1})$ graph. Taking into account that the 30-2 domain corresponds to the K_5 zonotope graph and the 30-3 domain corresponds to the $P_{24} + (K_5 - \mathbf{1})$ non zonotopal graph it is clear that going from domain 30-2 to the wall **28.96**-40 is a simple zone contraction graphically visualized as removing one edge. At the same time going from domain 30-3 to the same wall is not a zone contraction transformation. This transformation can be described as "elimination of the P_{24} contribution".

In a similar way going from the 30-4 domain to the wall **30** $-$ **102**-36 has the same type. This transformation is again associated with "elimination of the P_{24} contribution" and is not of a standard contraction type. All other walls between generic domains are of simple contraction type, which are graphically represented by removing one edge from the graph.

The comparison of graphical representations of zonohedral lattices (Figure 6.23) and non-zonohedral ones (Figure 6.22) clearly indicates that there are similar transformations with "elimination of the P_{24}-contribution" during passage from lower dimensional subcones to their walls. For example the non-zonohedral lattice **28.104**-24 represented as $P_{24} + (K_5 - 2 \times \mathbf{1})$ and filling a 9-dimensional subcone can have as one of its 8-dimensional boundaries the zonohedral lattice **24.78**-24 which is graphically represented as $(K_5 - 2 \times \mathbf{1})$. Going from $P_{24} + (K_5 - 2 \times \mathbf{1})$ to $K_5 - 2 \times \mathbf{1}$ is not of a zone-contraction transformation but the "P_{24} elimination".
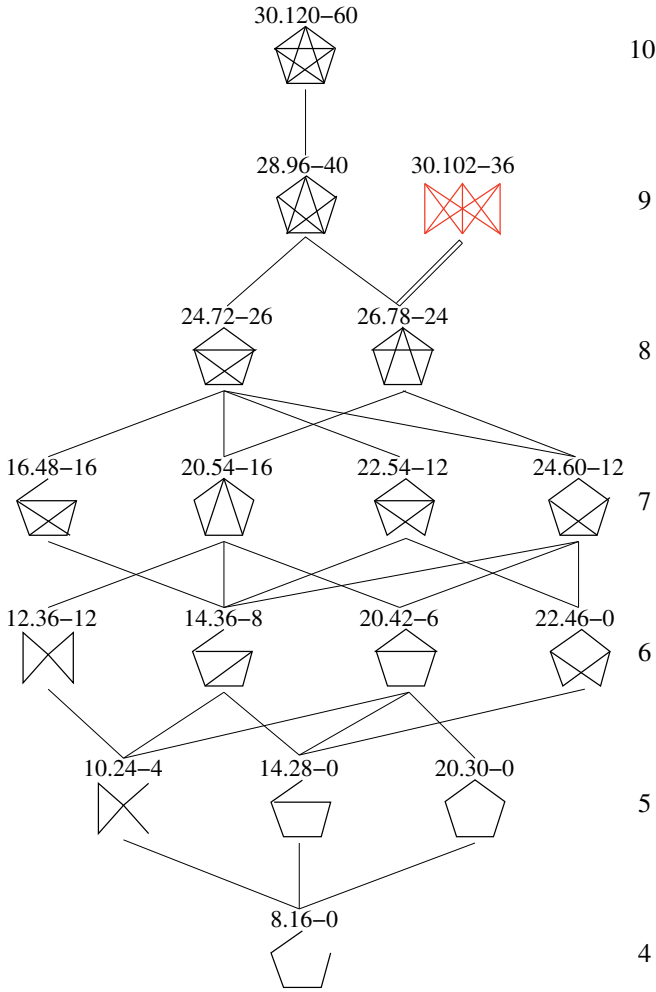
FIG. 6.23 – Graphical visualization of zonohedral four-dimensional parallelohedra.

To conclude the discussion of graphical representations of non zonohedral polytopes we note that this approach can be generalized to higher dimensional spaces. In order for the reader to follow this rather active direction of research we mention the recent paper [88] (and the most important of its predecessors [93, 38, 57, 58]). In [88] the description of six-dimensional polytopes represented in a form of $P_V(E_6) + Z(U)$ is studied. The $P_V(E_6)$ is the parallelotope associated with the root lattice E_6. (See chapter 7 of this book for an initial discussion of root lattices.)

6.9   On Voronoï conjecture

When discussing parallelohedra associated with facet-to-facet tiling of the space and corresponding lattice we have not stressed the difference between parallelohedra and Voronoï cells of lattices. It is clear that any Voronoï cell is a parallelohedron but the inverse is generally wrong.

In his famous paper [95] Voronoï formulated an important question: "Is an arbitrary parallelohedron affinely equivalent to the Dirichlet domain for some lattice?". Now the term "Dirichlet domain" is more often replaced by the "Voronoï cell" but the positive answer to this question is still absent and the affine equivalence between Voronoï cells of lattices and arbitrary parallelohedra is known as Voronoï's Conjecture.

Voronoï himself gave a positive answer to his question in the case when the parallelohedron P is primitive, i.e. when every vertex of corresponding tiling belongs to exactly $(d+1)$ copies of the d-dimensional parallelohedron P, or, in other words, each belts of P contains 6 facets. Since then, some progress has been made by extending Voronoï's Conjecture to a larger class of parallelohedra. The most serious steps are the following:

Delone [41] demonstrated that the conjecture is valid for all parallelohedra in dimensions $d \leq 4$.

Zhitomirskii [99] relaxed the condition of primitivity of parallelohedra for which Voronoï's Conjecture was proved to be valid. According to [99], a parallelohedron P is called k-primitive if each of its k-faces are primitive, i.e. every k-face of the corresponding tiling belongs to exactly $(d+1-k)$ copies of P. In particular, if each belt of P consists of 6 facets the parallelohedron is $(d-2)$-primitive. Zhitomirskii [99] extended the result of Voronoï on $(d-2)$-primitive parallelohedra.

Another class of parallelohedra for which the Voronoï's Conjecture was also proved [54] includes zonotopal parallelohedra.

Engel checked the Voronoï's Conjecture for five-dimensional parallelohedra by computer calculations [50, 51]. He enumerated all 179372 parallelohedra of dimension 5 and gave a Voronoï polytope affinely equivalent to each of the found parallelohedra.

Assuming the existence of an affine transformation that maps a parallelohedron onto a Voronoï polytope, Michel et al. [77] have shown that in the primitive case and in few other cases these mappings are uniquely determined up to an orthogonal transformation and scale factor.